

Citation for published version:
Tasso Guaraldo, T, Vakili, R, Wenk, J & Mattia, D 2023, 'Highly efficient ZnO photocatalytic foam reactors for micropollutant degradation', Chemical Engineering Journal, vol. 455, 140784. https://doi.org/10.1016/j.cej.2022.140784

10.1016/j.cej.2022.140784

Publication date: 2023

Link to publication

# **University of Bath**

#### **Alternative formats**

If you require this document in an alternative format, please contact: openaccess@bath.ac.uk

Copyright and moral rights for the publications made accessible in the public portal are retained by the authors and/or other copyright owners and it is a condition of accessing publications that users recognise and abide by the legal requirements associated with these rights.

**Take down policy**If you believe that this document breaches copyright please contact us providing details, and we will remove access to the work immediately and investigate your claim.

Download date: 09. Mar. 2023

# Highly efficient ZnO photocatalytic foam

# reactors for micropollutant degradation

- Thais T. Guaraldo, Reza Vakili, Jannis Wenk, and Davide Mattia\*
- 4 Department of Chemical Engineering, University of Bath, BA2 7AY, UK.
- 5 E-mail: d.mattia@bath.ac.uk

6

2

#### Abstract

8

9

10

11

12

13

14

15

16

17

18

19

20

21

22

23

24

25

26

27

The efficient removal of organic micropollutants, pharmaceuticals, pesticides, drugs, and others, remains an unsolved challenge in water treatment. Although photocatalysis has proven highly effective at degrading these substances, its largescale implementation has been so far hampered by technical and economic concerns. This work describes the development and characterization of novel highly efficient. self-supporting photocatalytic ZnO foams for the degradation of organic micropollutants. A systematic investigation of flow rate, catalyst length and stability under both recirculating and single-pass conditions was conducted using carbamazepine as a UV-recalcitrant model pollutant. Under recirculation, 95% degradation was achieved with photocatalyst quantum yield of 1.2×10<sup>-3</sup> and electrical energy per order (E<sub>EO</sub>) as low as 24 kWh m<sup>-3</sup>, values outperforming current technology, slurry and immobilised systems. For single-pass tests, complete degradation was achieved in 30 minutes, with the quantum yield increasing to 6.3×10<sup>-3</sup>, and an E<sub>EO</sub> of 36 kWh m<sup>-3</sup>. These values also outperform those for slurries, immobilised and other foam photocatalyst reported in the literature under similar conditions. The low energy consumption of these newly developed photocatalytic foams, combined with their high quantum yield and stability, provides a realistic path towards practical implementation of photocatalytic processes in water treatment, addressing the limitations of existing slurry and immobilised photocatalytic technology.

28

29

- Keywords: Photocatalytic Foams: Photocatalysis; Recirculation Reactor; Single Pass
- 30 Reactor; Energy Efficiency

#### 1. Introduction

Over 2 billion people lack access to safe drinking water and nearly half of the global population lacks access to safe sanitation [1]. Regulatory agencies around the world are particularly concerned with the increasing presence of organic micropollutants in water, with more compounds periodically added to watchlists or slated for removal [2]. In this context, novel water treatment technologies are needed to remove these micropollutants in an environmentally and economically sustainable way [3].

There is ample evidence of the effectiveness of photocatalysis at removing organic micropollutants and/or recalcitrant compounds from water or at least convert them into more readily biodegradable compounds [4]. However, large-scale implementation of photocatalysis within tertiary wastewater treatment schemes has been so far limited by technical and economic concerns [5]. In particular, high electrical energy per order (EEO) values and a low quantum yield for hydroxyl radicals limit the practical use of photocatalysts [6]. The most studied configurations for photocatalytic treatment are nanoparticle slurries and immobilised catalysts [7-9]. While the former are particularly efficient due to a high surface area, downstream catalyst removal is required. The latter address catalyst separation issues, but are limited by lower removal efficiencies and slower degradation kinetics as the active area is drastically reduced [5]. The post-recovery of photocatalysts remains the main technological challenge preventing commercialization and utilization of photocatalysis for wastewater treatment [10]. Further critical issues include long-term stability of photocatalysts, leaching and their overall cost-effectiveness ratio [11].

Photocatalytic foams are alveolar materials of open porosity with cells connected through struts to form a monolith. Foam 3D structures can be characterised using parameters such as pore diameter, strut diameter and cell size [12]. The

immobilisation of nanoparticles onto commercial foam supports has been used as an attempt to bridge the performance gap between slurries and immobilised catalysts [13-15]. Typical commercial foam supports include, but are not limited to, silicon carbide, alumina and metals (Ni, Cu) [12, 16-18]. Nanoparticles are primarily titanium dioxidebased, either as commercial P25 particles dip coated onto foams substrates [19-21] or prepared by sol-gel method [17, 22]. Recently, titania foams produced using a sequential multi-step coating approach were studied in batch reactors for reactive orange dye degradation [23], and diuron pesticide degradation under simulated solar irradiation [4]. ZnO structures hydrothermally deposited onto metallic [24] and carbon [15] foam supports studied Rhodamine B dye degradation under visible and UV light irradiation in batch reactors. Particle immobilising strategies include sequential multistep onto PU foam supports aiming at UV-mediated degradation [25], and the combination of metal oxide particles with Ag [26] and Ag<sub>2</sub>O [27] particles using metallic substrates for visible light batch systems. Although these foams with immobilised nanoparticles demonstrated superior photocatalytic efficiency compared photocatalytic slurries, the potential leaching of nanoparticles remains environmental concern and a challenge for large-scale industrial applications [9]. Furthermore, some of these systems showed a high energy consumption (> 2400 kWh m<sup>-3</sup>) even for dye degradation [27].

57

58

59

60

61

62

63

64

65

66

67

68

69

70

71

72

73

74

75

76

77

78

79

80

81

A potential alternative using substrate-free ZnO photocatalytic foams, where the photocatalytic activity is given by the foam material itself, with no nanoparticles present, was previously tested in small-scale batch experiments by the authors [28]. Considering large scale applications, ZnO is relatively inexpensive when compared to TiO<sub>2</sub> and can absorb more light quanta than other conventional photocatalysts [29]. The ZnO photocatalytic mechanism, involving the formation of electron/hole pairs

under irradiation during the degradation of organic micropollutants, is well established [29]. As an example, carbamazepine (CBZ) oxidation occurs via hydroxyl radicals into acridine (AI) and acridone (AO) products [30, 31]. Complete oxidation of CBZ, AI and AO was demonstrated for ZnO foams [28]. The use of oxygen saturated conditions significantly reduces the effects of photocorrosion, whereby photogenerated holes can attack the Zn-O bond, dissociating Zn<sup>2+</sup> [32].

The majority of studies on immobilised foams have been in batch, with few conducted under recirculating conditions: SiC and alumina foam supports coated with TiO<sub>2</sub> commercial nanoparticles were used for the removal of paraquat herbicide, tertiary amine and pyrimethanil pesticide under UV irradiation [21, 33, 34]. TiO<sub>2</sub> composite films deposited on polyurethane and aluminium foams via polymeric [35] and silica sol-gel combination [20] promoted photocatalytic UV mediated degradation of dyes and pesticides. With only limited results on the performance of photocatalytic foams under recirculating flow configurations, to the authors' best knowledge there are no studies on single-pass configurations, which would be closest to practical application in water treatment.

In this work, self-supporting, substrate-free, ZnO photocatalytic foams are presented to concomitantly address the need for downstream removal of nanoparticle slurries and poor efficiency of immobilised materials. Two reactor configurations were systematically investigated, recirculating and single-pass, a significant advancement over convectional batch testing, and a step towards implementing photocatalysis in real applications. Highly efficient self-supporting ZnO photocatalytic foams with high mechanical and chemical stability were developed to withstand high water flow, and fully characterised to link synthesis conditions, foam characteristics and photocatalytic performance, using CBZ as a model organic micropollutant. The choice of CBZ, a

major organic micropollutant worldwide [36], allowed direct comparison with the literature, revealing the foams' superior performance. CBZ was selected as a model compound due to its recalcitrance to direct photolysis under UV-irradiation [37] and because of its widespread use as a benchmark compound in photocatalytic research [38]. Modelling studies of the single pass reactor, based on experimental data provided, show the scale-up potential of the foams.

#### 2. Experimental

# 2.1. Materials

Polyvinyl alcohol (PVA) 87-89 % hydrolyzed, (molecular weight 13,000-23,000), phosphoric acid and nitric acid were purchased from Acros. The cross-linker 2,5-dimethoxy-2,5-dihydrofuran (DHF) and the cationic surfactant, hexadecyltrimethylammoniumbromide (CTAB) were supplied by Merck (Germany). ZnO powder (purity 99.9%; average particle size  $5.0~\mu m$ ) was supplied by Goodfellow. Methanol and acetonitrile were purchased from Fisher. CBZ was supplied by Sigma-Aldrich. Stock solutions of CBZ (1.0 mmol L-1) were stored at 4 °C and replaced monthly. All aqueous solutions were prepared using ultrapure water (Veolia Purelab Chorus, resistivity  $18.2~M\Omega$ ).

# 2.2. Photocatalytic foams synthesis

Photocatalytic foams were produced using a combination of liquid templating and sintering methods [28], with a novel two-step sintering process developed here to obtain sturdier structures for application in flow processes. Briefly, the liquid template was composed of a particle-polymer-surfactant suspension of ZnO, PVA and CTAB, 40, 5.0 and 0.9 wt%, respectively, in water. After the addition of the DHF cross-linker.

air was incorporated using a homogenizer (IKA, Ultra-Turrax T25 basic) for 4 minutes at 11,000 rpm. The obtained solid materials were sintered using a two-step process to refine the microstructure of the pre-foam material and improve mechanical stability to withstand high flow conditions while maintaining macro and microporosity [39, 40]. The conditions used were 950 °C for 0.5 h followed by 900 °C for 12 h, with 5.0 °C min<sup>-1</sup> heating and cooling rates under atmospheric and nitrogen saturated conditions.

# 2.3. Photocatalytic foams characterisation

The synthesised foams' crystallographic structure was studied in a STADI P XRD diffractometer (Cu radiation) in transmission mode for 2θ values between 20° and 80°. The effect of chemical stability was investigated using Inductively Coupled Plasma Mass Spectrometry (ICP-MS) in a Thermo Fisher Scientific X-Series II instrument. Standard deviation error for all samples did not exceed 5.0 %.

The photocatalytic foams morphology was analysed in a Jeol JSM-7900F FESEM along with statistical image analysis to obtain flake size distribution and particle size distribution using Image J software. The porosity was calculated using the following equation based on Archimedes' principle [41]:

$$\varepsilon_f = \frac{\frac{(\omega_1 - \omega_2)}{D_w}}{\left[\frac{(\omega_1 - \omega_2)}{D_w} + \frac{\omega_2}{D_f}\right]} \tag{1}$$

where  $\epsilon_f$  is the foam porosity;  $\omega_1$  is the weight of the wet foam (g);  $\omega_2$  is the weight of the dry foam (g);  $D_w$  is the water density (g cm<sup>-3</sup>) at 15 °C;  $D_f$  is the ZnO foam density (g cm<sup>-3</sup>).

Macrostructural information was obtained using micro computed tomography (micro-CT) performed using a Nikon XT H 225ST scanner. The conditions used for analysis were 0.708 seconds exposure, magnification axis 173.7, 170 kV voltage, 130  $\mu$ A current, no filter material, 18 gain and tungsten target. In total, 3141 projections (4 frames per projection) were obtained and averaged. Information was limited to the machine resolution of 20  $\mu$ m. Data analysis and 3D images were accessed using Avizo software. Each sample was probed in three different areas of the foam with the same internal volume (0.5 × 0.5 × 0.5 cm) to assess their homogeneity.

#### 2.4. Photocatalytic activity

152

153

154

155

156

157

158

159

160

161

162

163

164

165

166

167

168

169

170

171

172

173

174

175

176

Photocatalytic degradation of CBZ (10 µmol L<sup>-1</sup>) in ultra-pure water was studied in a recirculating flow reactor (Fig. 1A) with a reservoir of 500 mL maintained at 10 ± 1 °C using a water-cooled chiller (RC-10 digital VWR) and continuously stirred (ultra-flat IKA). The solution flow rate was controlled using a gear pump (MCP-Z Ismatec) in the range of 100 to 500 mL min<sup>-1</sup>. Solutions were saturated with oxygen for 40 min prior to experiments and continuing during the experiments to minimise the well-known zinc oxide photo-corrosion effect [32]. Additionally, solutions were maintained under recirculation (dark conditions) for 40 min to achieve the adsorption/desorption equilibrium. Photocatalytic foams were placed in a quartz tube (ID 22 mm; OD 25 mm) and irradiated coaxially by three UV lamps to provide a cohesive light intensity (Aquatix pond, 254 nm, 5 Watts, averaged irradiance  $I_{0\lambda} = 10.4$  mW cm<sup>-2</sup>  $\pm 0.4$  mW cm<sup>-2</sup>) measured regularly at multiple locations using a UVC radiometer (International Light Technologies-ILT 2400) at a fixed distance of 3.0 cm between catalyst and lamps and inside the quartz tube. The effect of flow rate (100 to 500 mL min<sup>-1</sup>), catalyst length (2.1, 4.2 and 6.3 cm) and stability (5 cycles of 2 hours each) were studied using this configuration for 2.0 hours. Adsorption of CBZ on foams and reactor surfaces was

negligible. Direct photo-transformation of CBZ was  $10.0\% \pm 1.2 \times 10^{-4}$  degradation within 2.0 hours.

The performance of photocatalytic foams was also studied in a single-pass configuration (Fig. 1B) to match actual operational conditions. This was done using the same irradiation system as previously described with a total catalyst length of 8.4 cm for all experiments. A syringe pump (Nexus 6000) of fixed volume controlled the flow rate in the range of 0.7 to 5.0 mL min<sup>-1</sup>. CBZ solutions were saturated with oxygen for 40 min prior to degradation experiments along with adsorption/desorption equilibrium under dark conditions. The system was pre-filled with solution prior to degradations and the total treated volume was 150 mL for all studied flow rates under these conditions. As the volume was fixed, photolytic and photocatalytic degradation experiments were performed for different times according to the selected flow rate. The number of data points was relative to the residence time. The metallic tube around the quartz in the reactor can act as light-reflecting surface maximising photocatalytic efficiency for both configurations [9].

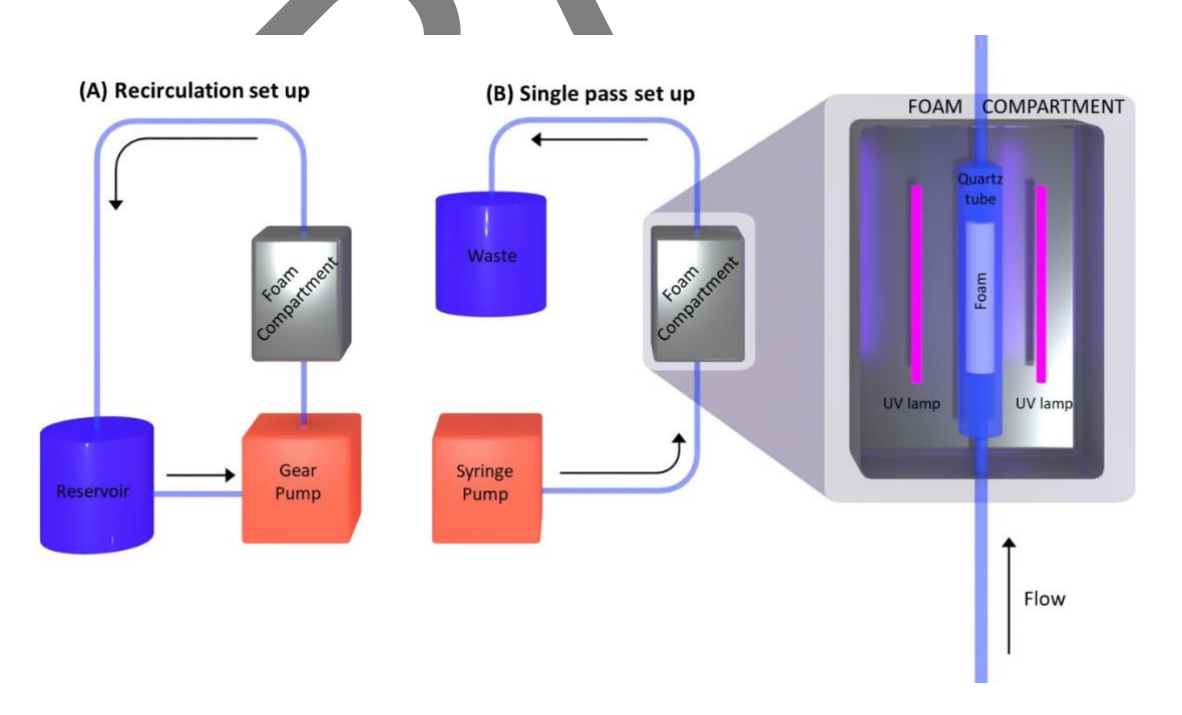


Fig. 1. Photocatalytic reactor in (A) recirculation and (B) single-pass configurations.

195

196

197

198

199

200

201

202

203

204

205

206

CBZ removal was monitored using high-performance liquid chromatography (Thermo Scientific Ultimate 3000 liquid chromatograph using a UV detector) equipped with a Thermo Scientific<sup>™</sup> Acclaim<sup>™</sup> 120 C<sub>18</sub> column (3.0 x 75 mm, particle size 3.0 µm), inclusive of a guard column, at a flow rate of 0.8 mL min<sup>-1</sup>, injection volume of 20 μL, detection wavelength 285 nm and mobile phase consisting of 5.0 mmol L<sup>-1</sup> phosphoric acid and acetonitrile 70:30 (v/v). The calibration curve was in the range of 0.1 to 25 µmol L-1. Aliquots were collected from either the reservoir (Fig. 1A) or the reactor outlet (Fig. 1B) at different time intervals.

The performance of the photocatalytic foams was initially evaluated as the percentage of removal (% R) per time. Pseudo-first order removal rate constants k (min<sup>-1</sup>) were calculated using linear regression of the logarithmic normalised concentration versus time:

$$% R = [1 - (C/C_0)] \times 100$$
 (2)  
 $ln(C/C_0) = -kt$  (3)

$$ln(C/C_0) = -kt (3)$$

207

208

209

210

211

212

where  $C_0$  is the initial concentration (µmol L<sup>-1</sup>), C is the final concentration (µmol L<sup>-1</sup>) and t is the reaction time (min).

Hydrodynamics calculations for the dimensionless numbers Reynolds (Re), Peclet (Pe), Schmidt (Sc) and Sherwood (Sh) considered flow in a tubular channel according to the equations below [42]:

$$Re_{D_h} = \frac{WD_p}{uA} \tag{4}$$

$$Pe = \frac{uD_p}{D} \tag{5}$$

$$Sc = \frac{\mu}{\rho D} \tag{6}$$

$$Sh = 1.029 * Sc^{0.33} * Re_{Dh}^{0.55} * \left(\frac{L}{D_p}\right)^{-0.472}$$
(7)

where  $D_p$  is diameter of pores (m), W is the mass flow rate (kg s<sup>-1</sup>), A is the tube cross sectional area (m²), u is the mean fluid velocity (m s<sup>-1</sup>),  $\mu$  is the dynamic viscosity of the fluid (kg m<sup>-1</sup>s<sup>-1</sup>),  $\rho$  is the density of the fluid (kg m<sup>-3</sup>) and L is the length of the foam (m). Intrinsic velocity corrections considered the difference between the empty and porous cylinders (V<sub>ext</sub> = V<sub>int</sub>\* $\epsilon$ ) [42]. The calculated parameters for recirculation and single-pass reactor configurations are in ESI Tables S6 and S7. The pressure drop along the foams was negligible (Table S11).

Correlations from photocatalytic degradation of CBZ were evaluated statistically using Pearson's correlation coefficient (Pearson's r). The trendlines used for the graphs were based in the piecewise polynomial function named as  $\beta$ -spline provided by Origin software.

# 2.5. UV dose, quantum yield and energy efficiency calculations

The UV dose was calculated for each degradation setup considering the attenuated irradiance  $I_{\alpha\lambda}$  ( $Wm^{-2}$ ) reaching the foam (equation S1 ESI), using the definitions in the IUPAC glossary for photochemistry [43]:

$$UV \ dose_{single \ pass} = \tau \times I_{\alpha\lambda} \tag{8}$$

$$UV\ dose_{recirculating} = n\tau \times I_{\alpha\lambda} \tag{9}$$

$$\tau = \frac{V_R}{Q}; \ n = \frac{t}{V_0/Q}; \ V_R = \varepsilon_f V_f \tag{10}$$

where  $\tau$  is the residence time under UV within the foam (s); n is the number of recirculation cycles,  $V_R$  is the volume receiving UV dose (mL),  $V_0$  is total reaction solution (mL),  $\varepsilon_f$  is the porosity of the foam and  $V_f$  is the volume of the foam (m³). Table S3 (ESI) shows the residence time, total time under UV number of cycles, and the fraction of volume illuminated over total volume (V<sub>illuminated</sub>/V<sub>0</sub>) for each reactor configuration. It is noted that while in the single pass configuration the UV dose is a function of flow rate, this is not the case in the recirculation experiments. UV doses are reported in Tables S4 and S5 (ESI).

The apparent quantum yield (Φ) was calculated considering equations S3 to S11 described in ESI, and is defined as the ratio of the reaction rate (mol s<sup>-1</sup>) to the photon flux (mol s<sup>-1</sup>) impinging on the photocatalyst/solution interface [43]. Calculations were performed considering light attenuation by the quartz tube (as light intensity was measured inside the tube) and at the liquid/solid interface due to water and CBZ (equation S1 ESI). Light-scattering losses in air were assumed negligible [19]. Calculations assumed all remaining photons were absorbed by the foams. Details of the calculations are described in the equations S3 to S12 ESI [28].

Electrical energy per order (E<sub>EO</sub>) was calculated according to the equations for the recirculating and single-pass reactors, respectively [44, 45]:

$$E_{EO} = \frac{P \times t}{V \times \log \left( {^{C_0}/_C} \right)} \tag{9}$$

$$E_{EO} = \frac{P}{Q \times log\left(\frac{C_0}{C}\right)} \tag{10}$$

where P is the lamp power (kW), t is the time (h), V is the treated volume (m³), C₀ and C the initial and final concentrations of contaminants (mol L⁻¹) and Q the flow rate (m³ h⁻¹). As the foams have different lengths, the lamp power value used in the above

equations is corrected for the effective length of the foams. As the foam occupied only a fraction of the quartz tube, the total power of the lamps was multiplied by the volumetric fraction occupied by the foam, to provide the effective power used for photocatalysis, considering that the contribution of photolysis is negligible. Details of the calculations are provided in the equation S10 ESI.

All information related to modelling and simulation is presented in the ESI section 2.

# 3. Results and discussions

#### 3.1. Photocatalytic foams characterisation

The novel two-step sintering process introduced here led to the formation of self-supporting ZnO photocatalytic foams (Fig. 2a) which are highly porous (93.0-94.0%), yet significantly more robust compared with the one step process previously demonstrated [28], The micro-CT showed the presence of large, interconnected pores with mean diameter of 540  $\pm$  18.3  $\mu$ m (Fig. 2b,c). The walls of the foams consist of porous 2D flakes (Fig. 2d) which, in turn, consist of sintered particles (Fig. 2e). The flakes have a mean size of 9.0  $\mu$ m (Fig. 2f) while the average particle size within the flakes is 2.1  $\pm$  0.6  $\mu$ m (Fig. 2g). Voids were formed internally in the flakes structure with mean size distribution of 0.58  $\pm$  0.19  $\mu$ m (Fig. 2e) in agreement with previous reports on ZnO [46]. The wurtzite crystal structure and improved crystallinity over ZnO particles precursor (Fig. S1 and Table S1 ESI) were confirmed by XRD.

The two-step sintering process yielded more robust foams via pore wall densification, which was achieved through pre-coarsening of the structure at higher temperature while simultaneously retaining residual macroporosity during the second

sintering stage [47]. After the sintering process, a band gap value of 3.26 eV was measured, in line with previous reports [48, 49].

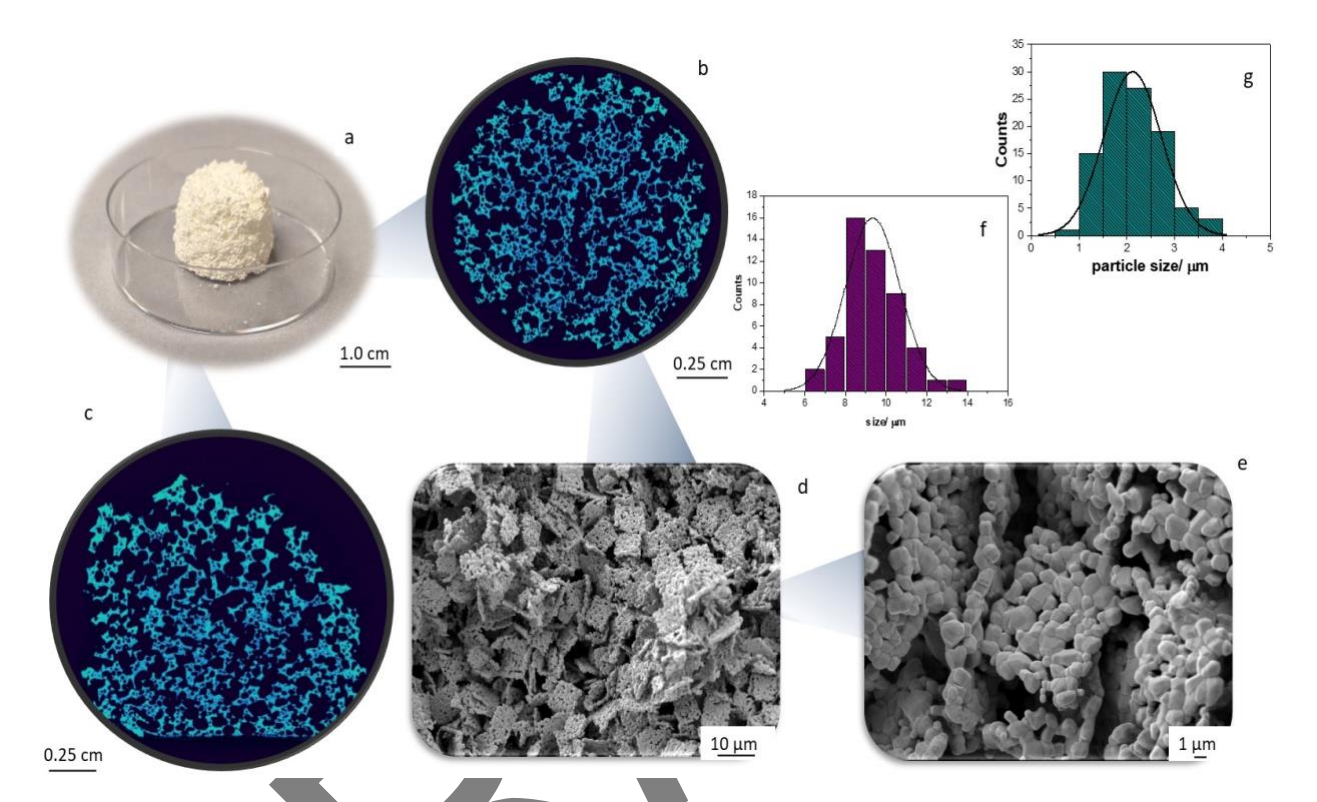


Fig. 2. ZnO foams (a) optical image, micro-CT reconstruction of the internal porous structure (b) top slice view (c) and lateral slice view. FESEM micrographs of (d) pores walls and (e) walls with higher resolution; (f) flake and (g) particle size distribution, both obtained from image J software.

# 3.2. Photocatalytic activity: recirculating system

Photocatalytic degradation of CBZ under recirculation conditions shows 66 and 64 % removal for the ZnO foams sintered under atmospheric and nitrogen saturation conditions after 2.0 hours at 200 mL min<sup>-1</sup>, respectively (Fig. 3A). The contributions of adsorption and photolysis were less than 10% combined (Table S2 ESI), lower than

what observed for similar foams in a batch reactor for the same reaction time (~14%) [28]. This was further confirmed by calculating the quantum yield, with values of  $3.6 \times 10^{-6}$  in the absence of the catalyst (photolysis) and  $4.5 \times 10^{-4}$  and  $3.5 \times 10^{-3}$  in the presence of photocatalytic foams, under atmospheric and nitrogen saturation respectively (Table S2 ESI). Lower quantum yields were obtained for foams sintered under nitrogen saturation (Table S2 ESI). The photolysis quantum yield was lower than reported value of 6.0×10<sup>-4</sup> mol Einstein<sup>-1</sup> for CBZ photochemical degradation [37, 50]. Compared to a similar foam in a batch reactor, the recirculating system had 3 and a half times faster kinetics to reach the same percentage degradation [28]. Furthermore, significantly lower UV doses were needed to promote CBZ photocatalytic degradation in the recirculating reactor. Comparing the UV dose of batch [28] and recirculating configurations, the latter demonstrated significantly higher efficiency of 66 vs 3 % for the lowest batch UV dose (Fig. S2 ESI). CBZ and intermediates (acridine and acridone) degradation was also demonstrated by increasing the degradation time [28]. Hydroxyl and superoxide free radicals are generally responsible for ZnO photocatalytic activity. Under irradiation, reactive oxygen species (ROS) are formed, in particular superoxide (O<sub>2</sub>-), associated to the presence of ZnO facets (0001) (Fig. 2e) [51].

292

293

294

295

296

297

298

299

300

301

302

303

304

305

306

307

308

309

310

311

312

313

314

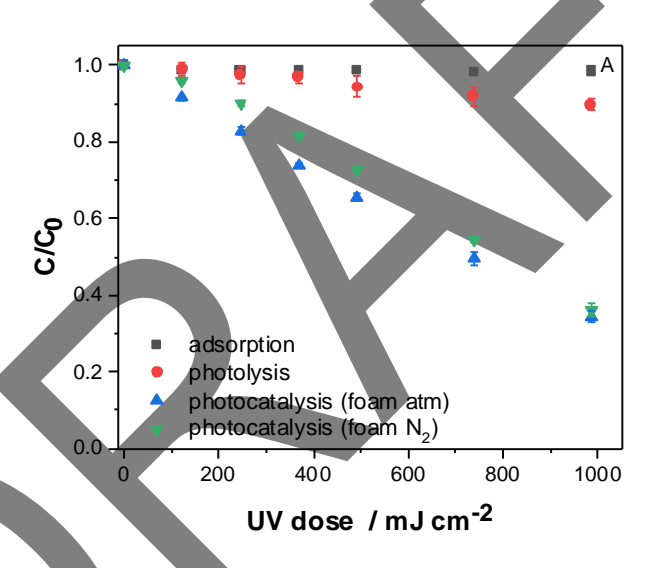
315

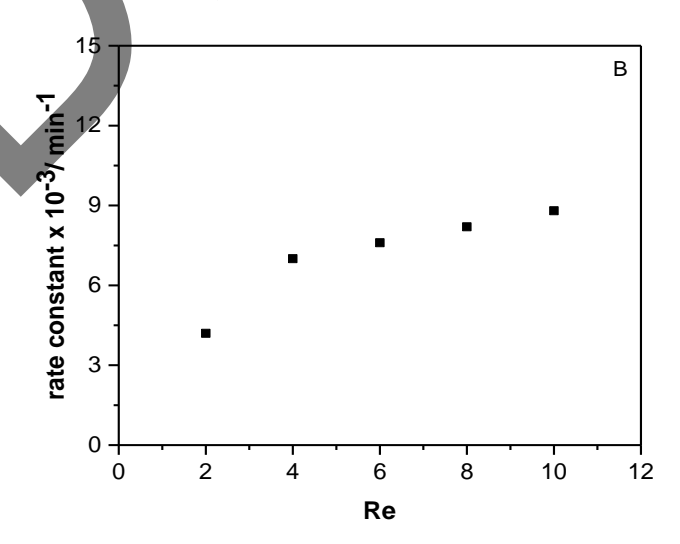
316

Based on this initial set of results, the recirculating photocatalytic reactor was modelled assuming a cubic cell model, and strut diameter (d<sub>s</sub>), cell dimension (a) and porosity data from experimental values. The model showed a high correlation between the experimental data and modelling (Fig. S5 and Fig. S6 ESI), and the degradation reaction of at first order type (Fig. S7 ESI). Fluid dynamics parameters relative to the heat and mass transfer were calculated as Sherwood number (Sh) and Nusselt number (Nu). The modelling then considered a range of flow rates from 100 to 500 mL

min<sup>-1</sup>, showing the reaction rate strongly depends on the flow rate up to 200 mL min<sup>-1</sup>. Above 200 mL min<sup>-1</sup>, the reaction rates were substantially invariant (Fig. S8 ESI), allowing to consider the system free from solid–liquid mass transfer resistances.

As numerous photoactivated processes are occurring simultaneously and there are multiple materials and process parameters affecting the degradation, the quantum yield was calculated against key materials properties of the foams, surface area (SA) and surface area-to-volume (SAV) ratio, to assess their individual effects (Table S2 ESI). SAV showed the best correlation, as it incorporates the content of material present as SA, given porosity and interconnected pore size, within the total volume.





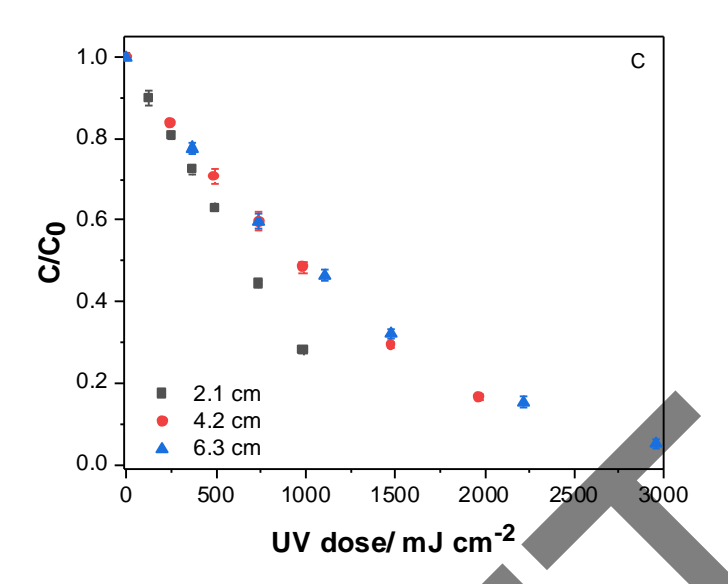


**Fig. 3.** (A) Degradation of CBZ by (■) adsorption, (•) photolysis and photocatalysis using foams sintered under (▲) atmospheric and (▼) nitrogen saturated conditions. Flow rate 200 mL min<sup>-1</sup>. Photocatalytic degradation of CBZ (C/C<sub>0</sub>) using ZnO foams as a function of UV dose for (B) different flow rates and (C) different catalyst lengths at 300 mL min<sup>-1</sup>.

# 3.2.1. Operational and structural parameters: flow rate, catalyst length effect and UV dose and catalyst length

A systematic analysis of operational and structural parameters was conducted to optimise the foams' performance. Significant changes in CBZ photocatalytic degradation kinetics were observed as a function of flow rate with strong linear correlations, from 100 to 500 mL min<sup>-1</sup> (cross ref Table 1 and Fig. 3B), due to hydrodynamics effects. As the flow rate increased, the residence time decreased and number of cycles progressively increased (Table S3 ESI), resulting in constant UV doses. Across all flow rates tested, the reactor is in laminar flow regime ( $2 \le \text{Re} \le 10$ , Fig. 3B). As the flow rate increased from 100 to 200 mL min<sup>-1</sup>, kinetics more than

doubled, typical of a mass transfer-limited regime. The increase can be attributed to a decrease in the thickness of the boundary layer, leading to improved mass transfer [52]. Above 200 mL min<sup>-1</sup>, there is only a weak dependence of kinetics on flow rate (Fig. 3B), with degradation being adsorption controlled. A Peclet number (the ratio of diffusion time over convection time), Pe >1, for all flow rates and a doubling of the Sherwood number (the ratio of convective mass transfer rate over diffusion rate), Sh from 3 to 7, further confirm this analysis. Conversely, Sh halved from 6 to 3 with increased catalyst length for a fixed flow rate. All calculated parameters are reported in the Table S6 ESI. The complex effect on photoactivity of hydrodynamic conditions can be attributed to the highly porous structure of the foams (> 90%) with heterogeneous interconnected pores of different diameters (Fig. 2). Similar effects have been observed in porous media [53], where convective mass transfer dominates within the macroscopic interconnected pores, and diffusion, adsorption and desorption dominate in the smaller pores surrounding the large ones [54], and within the porosity of the foam walls. To the best of the authors knowledge, similar comparisons for foams in recirculation reactors had not yet been reported.

ZnO foams were highly photoactive under recirculating conditions and UV irradiation since the right combination of the foams' properties (pore diameter, SAV and porosity) led to higher light penetration across the 3D catalyst structure. Strong correlations were observed between photocatalytic degradation kinetics, flow rate and foam length under recirculating conditions (cross ref. Fig. 3b-c, Table 1 and Fig. S3 ESI). Additionally, a high linear inverse correlation (< -0.800) was obtained for flow rate and electrical energy per order (E<sub>EO</sub>), with the latter reducing as the former increases. Kinetics and quantum yield linearly increased with catalyst length underpinned by strong correlations. 95% CBZ removal was achieved by tripling the

foam's length after 2.0 h with quantum yield of  $1.2 \times 10^{-3}$  (Table 1). Normalised numbers demonstrated the SA remained constant (correlation -0.866,  $R^2 = 0.432$ ) while a strong correlation with the surface-to-volume ratio (SAV) was obtained (0.986,  $R^2 = 1.0$ ).

**Table 1.** Quantum yield  $(\Phi)$  and normalised quantum yield considering the foams' properties of surface area (SA) and surface area to volume (SAV) as a function of flow rate, catalyst length, % CBZ removal, pseudo first order removal rate constant (k) and electrical energy per order (EEO) for recirculating reactor along with correlations.

Flow rate	Catalyst length (cm)	%CBZ removal	k		norma	_ E <sub>EO</sub>	
(mL min <sup>-1</sup> )			(s <sup>-1</sup> )*	Φ (-)	Φ/ŚA (m <sup>-2</sup> )	Φ/SAV (m)	(kWh m <sup>-3</sup> )
100		45.0	7.0×10 <sup>-5</sup>	2.7×10 <sup>-4</sup>	0.9×10 <sup>-2</sup>	6.4×10 <sup>-8</sup>	40
200		66.0	1.2×10 <sup>-4</sup>	4.5×10 <sup>-4</sup>	1.5×10 <sup>-3</sup>	1.1×10 <sup>-7</sup>	22
300	2.1	72.0	1.3×10 <sup>-4</sup>	4.9×10 <sup>-4</sup>	1.6×10 <sup>-3</sup>	1.2×10 <sup>-7</sup>	19
400		72.0	1.4×10 <sup>-4</sup>	5.3×10 <sup>-4</sup>	1.7×10 <sup>-3</sup>	1.3×10 <sup>-7</sup>	19
500		76.0	1.5×10 <sup>-4</sup>	5.7×10 <sup>-4</sup>	1.9×10 <sup>-3</sup>	1.3×10 <sup>-7</sup>	17
correlation	-	0.869	0.914	0.925	0.923	0.876	-0.820
	2.1	72.0	1.3×10 <sup>-4</sup>	4.9×10 <sup>-4</sup>	1.6×10 <sup>-3</sup>	1.2×10 <sup>-7</sup>	19
300	4.2	84.0	2.0×10 <sup>-4</sup>	7.8×10 <sup>-4</sup>	1.3×10 <sup>-3</sup>	1.8×10 <sup>-7</sup>	26
	6.3	95.0	3.2×10 <sup>-4</sup>	1.2×10 <sup>-3</sup>	1.3×10 <sup>-3</sup>	2.9×10 <sup>-7</sup>	24
-	correlation	0.999	0.989	0.995	-0.866	0.986	0.693

<sup>\*</sup> the associated error is < 10<sup>-3</sup>.

An extensive comparison of photocatalytic degradation of CBZ in the literature shows that the foams produced here outperform most nanoparticle suspensions and immobilised catalysts (Table 2): Nanoparticles suspensions in batch reactors achieved 1 to 4 orders of magnitude lower quantum yields than photocatalytic foams, e.g.  $4.6 \times 10^{-8}$  to  $2.6 \times 10^{-4}$  for TiO<sub>2</sub> under UV irradiation with significantly higher E<sub>EO</sub> values (34.3 to  $1.2 \times 10^{3}$ ) [55-57] and TiO<sub>2</sub> under LED [58]. The photocatalytic foams outperformed also ZnO and ZnO/biochar nanoparticles under UV irradiation in batch

Φ calculated using equation S7.

 $<sup>\</sup>Phi$ /SA and  $\Phi$ /SAV calculated using equations S8 and S9.

reactors [56, 59] considering both quantum yield and energy consumption (cross ref Table 1 and Table 2). While slightly higher quantum yields were reported for ZnO NPs under UV and visible irradiation [60-62] and even a nanoparticle composite of graphene oxide and Bi<sub>2</sub>O<sub>2</sub>CO<sub>3</sub> under simulated visible irradiation [60], energy consumption was higher by at least two orders of magnitude for CBZ photocatalytic degradation. A further comparison with foams of different materials, different reaction configurations and targeting a wide range of pollutants (Table S8 ESI) also showed the superior performance of the foams prepared in this work. TiO2 foams in batch reactors demonstrated lower quantum yields of 5.2×10<sup>-5</sup> (TiO<sub>2</sub>/βSiC) [4], 3.9×10<sup>-4</sup> (TiO<sub>2</sub>) [63], however had 2-3 orders of magnitude higher electrical energy per order when compared to the ZnO photocatalytic foams (cross ref Table 1 and Table S8 ESI). A 1-2 orders of magnitude lower quantum yield was reported for ZnO/rGO composite foam in a batch reactor [64], and for TiO<sub>2</sub>/Al foam in a batch recirculating reactor [17]. Apart from a similar ZnO foam under UV illumination in a recirculating system [65], all other foams demonstrated superior energy consumption ranging from 1.4×10<sup>2</sup> to 6.2×10<sup>4</sup> kWh m<sup>-3</sup> (cross ref Table 1 and Table S8 ESI). Increased quantum yield suggests ZnO photocatalytic foams enhanced the absorption of photons when compared to NPs suspensions and immobilised photocatalysts. Quantum yields obtained for ZnO photocatalytic foams were comparable to other AOPs as UV/H<sub>2</sub>O<sub>2</sub> (3.3×10<sup>-3</sup> mol Einstein<sup>-1</sup>) for CBZ degradation [66]. These results convincingly show that the use of photocatalytic foams in flow reactors could pave the way for enhanced light efficient and mass transfer photocatalytic

414

390

391

392

393

394

395

396

397

398

399

400

401

402

403

404

405

406

407

408

409

410

411

412

413

processes.

416 **Table 2.** Quantum yield  $(\Phi)$  and electrical energy per order  $(E_{EO})$  calculated for CBZ 417 degradation for different photocatalysts in batch, batch recirculating and flow reactors.

Photocatalyst	Material	Reactor	Irradiation (type, power, λ (nm))	Ф	E <sub>EO</sub> (kWh m <sup>-3</sup> )	Ref
	TiO <sub>2</sub>	Batch	UVA; 9W; 365 max	2.6×10 <sup>-4</sup>	34.3	[55]
	TiO <sub>2</sub>	Batch	UV; 150W; ≤300 max	-	92	[67]
	TiO <sub>2</sub>	Batch	UVA; 150W; 365 max	6.8×10 <sup>-6</sup>	170	[56]
	$C-TiO_2$	Batch	UVA; 150W; 400 max	4.6×10 <sup>-8</sup>	1,200	[57]
	$TiO_2$	Batch	LED vis; 417	6.9×10 <sup>-9</sup>	-	[58]
Suspensions	*g-C <sub>3</sub> N <sub>4</sub>	Batch	LED vis; 417	6.9×10 <sup>-7</sup>	-	[58]
	ZnO	Batch	UVA; 48W; 365	1.7×10 <sup>-2</sup>	320	[61]
	ZnO	Batch	UV; 150W; ≤300 max	-	260	[67]
	ZnO	Batch	UVA; 150W; 365 max	1.6×10 <sup>-5</sup>	210	[56]
	ZnO	Batch	Xe lamp; 5000W; 483	3.5×10 <sup>-3</sup>	22,000	[62]
	ZnO/biochar	Batch	UV; 90W; 365	4.0×10 <sup>-6</sup>	34,000	[59]
	**Bi <sub>2</sub> O <sub>2</sub> CO <sub>3</sub> /GO	Batch	Xe lamp; 300W; ≥365	2.6×10 <sup>-2</sup>	6,700	[60]
Immobilised	TiO <sub>2</sub>	Batch	Xe lamp; 55W; ≥365	3.8×10 <sup>-7</sup>	11,000	[68]
	$N-TiO_2$	Batch	Xe lamp; 150W; 480	-	14,000	[69]
	TiO <sub>2</sub>	Recirculating	UVA; 75W; 365	-	1,200	[70]
	TiO <sub>2</sub>	Flow	UVA; 300W; 365	-	0.07	[70]
	TiO <sub>2</sub>	Flow	UVA; 300W; 365 max	3.6×10 <sup>-5</sup>	3.3	[71]
	$N-TiO_2$	Flow	UVA; 300W; 365 max	7.7×10 <sup>-5</sup>	0.9	[71]
Foams	ZnO	Batch	UV; 5W; 254	3.6×10 <sup>-2</sup>	140	[28]
	ZnO	Recirculating	UV; 15W; 254	8.7×10 <sup>-4</sup>	21	[65]
Fuailis	ZnO	Recirculating	UV; 15W; 254	1.2×10 <sup>-3</sup>	24	This wo
	ZnO	Flow	UV; 15W; 254	6.3×10 <sup>-3</sup>	36	This wo
*graphitic carl	bon nitride; **graph	nene oxide (GO)				

# 3.2.2. Energy efficiency

415

419

420

421

422

423

424

425

426

427

A widely used measure of efficiency is electrical energy per order (E<sub>EO</sub>), defined as the kilowatt hours of electrical energy needed to decrease the concentration of a contaminant by one order of magnitude (90%) in one cubic meter of solution [45]. In general, the photocatalytic degradation of organic and inorganic pollutants is classified as a high energy process, with median E<sub>EO</sub> values of 335 kWh m<sup>-3</sup> for both suspensions and immobilised (TiO<sub>2</sub>, ZnO and WO<sub>3</sub>) photocatalysts, whereas other advanced oxidation processes (AOPs, e.g. ozonation based, UV/CI and UV/H<sub>2</sub>O<sub>2</sub>) have been considered more energy efficient (E<sub>EO</sub> < 10 kWh m<sup>-3</sup>) [6]. In the present work, the E<sub>EO</sub> of the foams ranged from 40 to 17 kWh m<sup>-3</sup>, with increasing flow rate (Table 1), significantly lower than the median for general photocatalytic processes. A more specific comparison with the literature limited to the photocatalytic degradation of CBZ, revealed that the foams produced here have the lowest E<sub>EO</sub> value, outperforming both suspensions and immobilised TiO<sub>2</sub> and ZnO catalysts (Table 2). Although the energy consumption was lower for some immobilised TiO<sub>2</sub> under UV [70, 71] irradiation in flow reactors, CBZ was not fully degraded under these conditions, reaching only 62% after 7 days (Table 2).

A further comparison with a wide range of AOPs for the degradation of CBZ showed that the low value of E<sub>EO</sub> of 24 kWh m<sup>-3</sup> is competitive with a wide range of AOPs both in batch and flow configurations, with only a few specific systems outperforming the foams produced here (Table S9 ESI).

These results clearly show that the combination of a flow reactor with the use of 3D photocatalytic foams resulted in significantly improved energy efficiency of this photocatalytic process compared to suspended and immobilised conventional photocatalysts.

# 3.2.3. Stability and reuse of foams

ZnO photocatalysts suffer from photocorrosion upon UV irradiation when oxygen is depleted [72]. The stability of substrate-free ZnO photocatalytic foams, in terms of Zn photo-corrosion [32], decreased with increasing flow rate (Fig. 4b). Zn<sup>2+</sup> release increased proportionally with foam length as more material was present in the reactor (Fig. 4b-c). Greater chemical stability was associated to lower flow rates (Fig. 4b). The photocatalysts were stable over 10 h (5 cycles of 2 hours each) under recirculating conditions at 300 mL min<sup>-1</sup> without any significant change in mass (Fig.

4a), nor in morphology (Fig. S4 ESI), before and after each cycle. The increase in zinc concentration is more pronounced from the first to the second cycle followed by a plateauing of values. Zn<sup>2+</sup> concentration in solution did not exceed 170 ppb per cycle (Fig. 4a). In terms of degradation process influence, a less pronounced corrosion effect was observed under dark conditions. Adsorption alone was responsible for approximately a third (20 ppb) of zinc concentration after 2.0 h for foams (2.1 cm) sintered under atmospheric conditions and a quarter for nitrogen saturated sintered foams (Fig. 4d). Foams prepared under nitrogen saturation had a slightly lower chemical stability (60 ppb) as opposed to atmospheric conditions (40 ppb) after 2.0 h of photocatalysis ((Fig. 4d). Numbers were significantly lower than maximum recommended zinc levels for drinking water of 3.0 ppm [73]. The stability of the substrate-free ZnO foams under recirculation presented here outperformed comparable systems in the literature, e.g. ZnO nanostructures immobilised onto Ni foams [24, 26] in terms of time on stream, or batch-wise Au/ZnO/rGO foams [13, 24, 26], in terms of performance stability. The chemical stability (Zn<sup>2+</sup> concentration) was not monitored for previously reported materials, so a direct comparison is not possible. All the photocatalytic foams retained their macroscopic integrity after

453

454

455

456

457

458

459

460

461

462

463

464

465

466

467

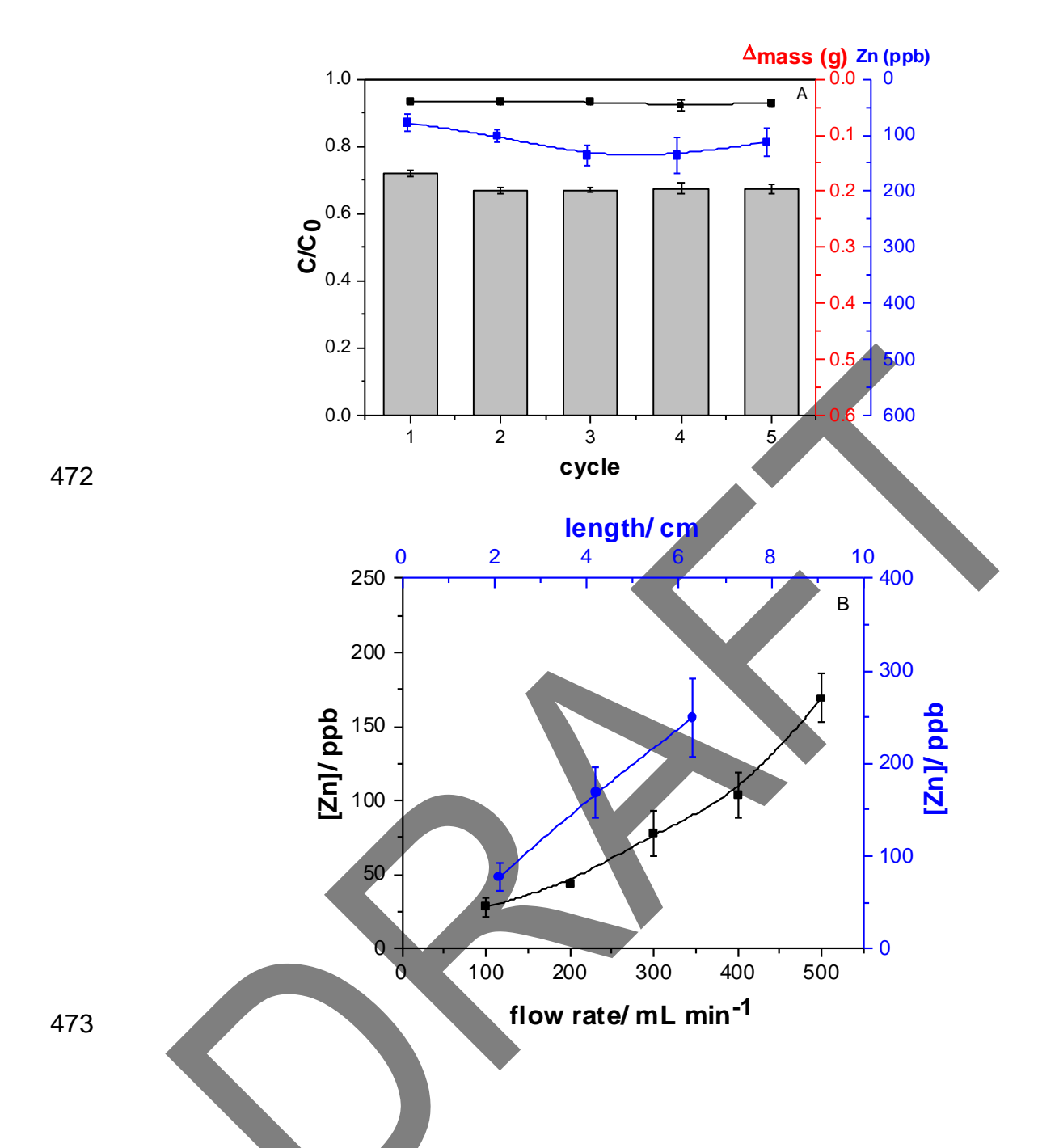
468

469

470

471

All the photocatalytic foams retained their macroscopic integrity after degradation experiments. Taken together, these findings confirm the effectiveness of the two-step sintering to improve the foams' mechanical and chemical stability.



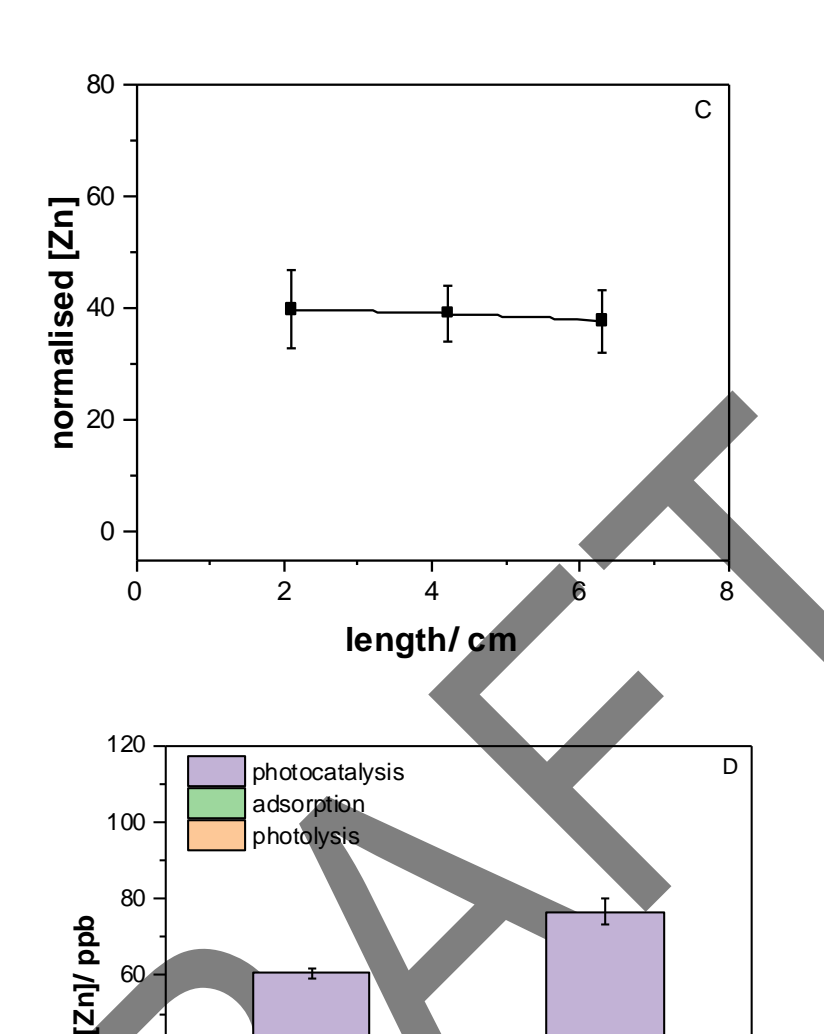


**Fig. 4.** Chemical stability of the ZnO foams for CBZ removal vs (A) reusability after 5 consecutive cycles of 2 hours each at 300 mL min<sup>-1</sup>; (B) flow rate and length of catalyst at 300 mL min<sup>-1</sup>; (C) zinc concentration normalised over catalyst length; and (D) influence of photolysis, adsorption and photocatalysis, as described in Fig.3a (200 mL min<sup>-1</sup>), on the overall stability.

photocatalysis (atm)

photocatalysis

 $(N_2)$ 

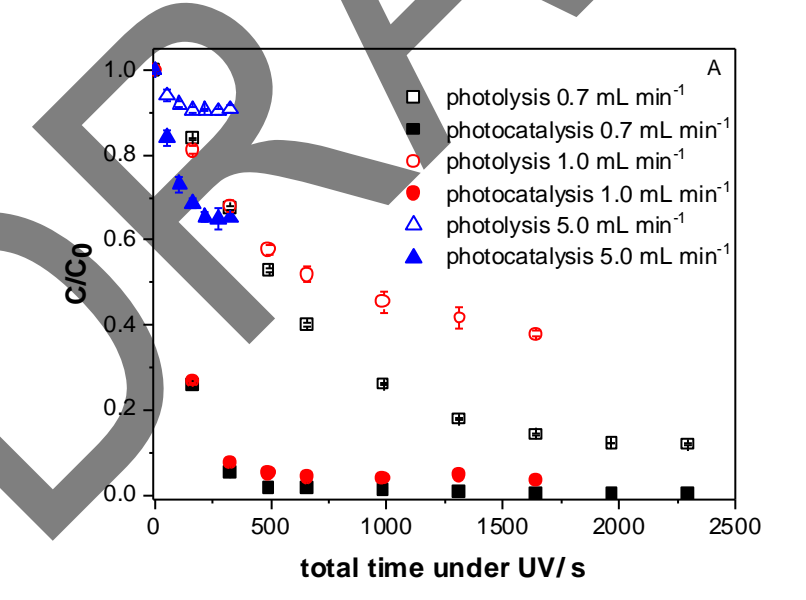
#### 3.3. Photocatalytic activity: single-pass reactor

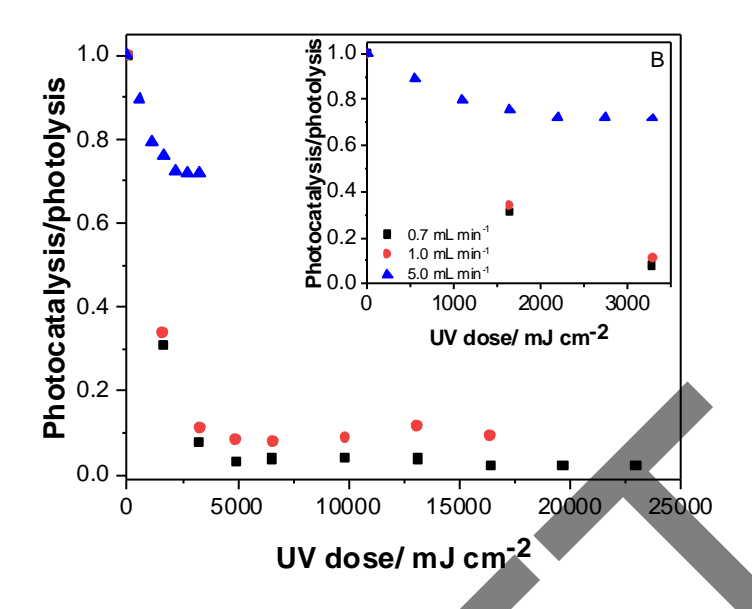
To further understand the scale-up potential of the substrate-free foams, single-pass experiments were conducted to mimic what would happen in actual wastewater treatment plants for both economic and practical reasons [52]. Single-pass tests were conducted using the substrate-free ZnO photocatalytic foams (total length of 8.4 cm compared to 6.3 cm in the recirculating case) at the range of 0.7 to 5.0 mL min<sup>-1</sup> flow rate for 10 µmol L<sup>-1</sup> CBZ solutions under UV irradiation (Fig. 5). Fig. 5a provides CBZ degradation for each studied flow rate condition with the respective photolysis control. As photochemical degradation was more pronounced at lower flow rates for all conditions, the photocatalysis to photolysis rate was plotted to show photocatalysis contribution only (Fig. 5b). Despite differences in residence time, similar UV doses were obtained for the different flow rate conditions (Fig. 5b) after 30 min of reaction. Fig. 5c shows the degradation kinetics as a function of Reynolds number for each flow rate along with zinc concentration measured after each experiment. Single-pass experiments were conducted at fixed volume of solution. Therefore, total degradation time was selected according to the residence time for each studied flow rate.

Single-pass degradations demonstrated a decrease in concentration with degradation time until steady-state levels (Fig. 5a), as opposed to a linear decay under recirculating conditions at higher flow rates (Fig. 3b). CBZ photocatalytic degradation reached 100.0 and 96.5% for both 0.7 and 1.0 mL min<sup>-1</sup> conditions, respectively, after only 30 min (cross ref Fig. 5a,b). A similar profile was reported previously for a continuous-flow reactor operating at 2.7 mL min<sup>-1</sup> with immobilised TiO<sub>2</sub>, although this required significantly longer time (200 min) [70]. By increasing the flow rate to 5.0 mL min<sup>-1</sup>, a different trend in degradation was observed with lower removal efficiency (35.0%) as residence time is significantly lower (Table S3 ESI). Higher flow rates

yielded a lower contribution of photolysis within the initial degradation stages until a plateau was reached (Fig. 5a,b). This contribution was more evident for 0.7 and 1.0 mL min<sup>-1</sup> conditions, as UV doses meaningfully increased (Table S5 ESI). The UV dose was comparable for all studied flow rates after 30 min of photocatalytic degradation (cross ref Fig. 5b and Table S5 ESI). These results suggest ZnO photocatalytic foams were highly photoactive at UV doses up to 3282 mJ cm<sup>-2</sup> and extended residence times (Fig. 5b inset). Photolysis alone could not fully degrade CBZ, with degradation kinetics improved by 1.6 to 5.1 times in the single-pass reactor compared to the recirculating reactor (cross ref Table 1 and 3). As increased kinetics were obtained for lower flow rates (Re < 1.0), chemical stability remains below WHO recommended levels of 3.0 ppm [73]. The Peclet number was well above unity, with Sh being below unity and increasing with increasing flow rate (Table S7 ESI).







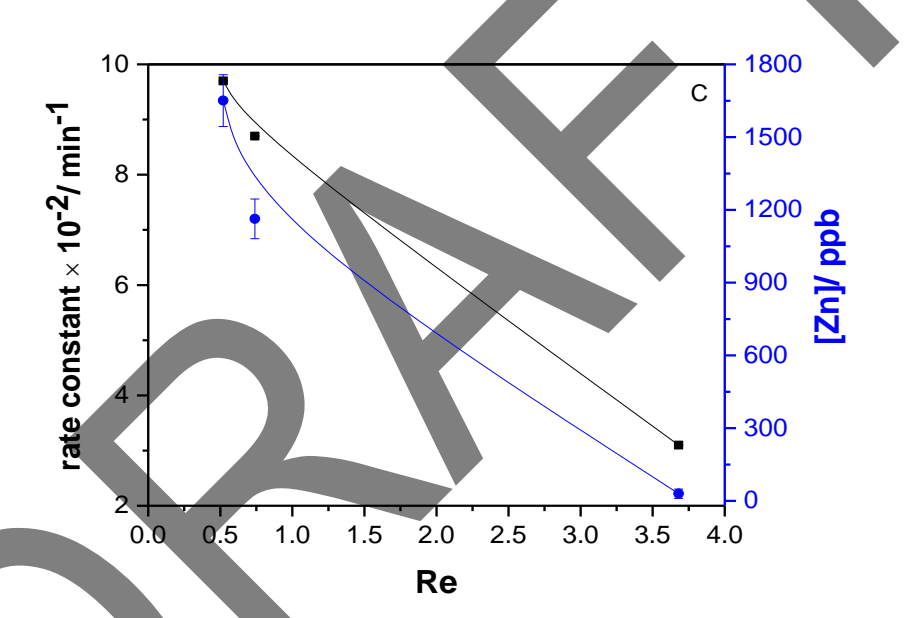


**Fig. 5.** (A) CBZ photocatalytic (closed symbols) degradation and correspondent photolytic (open symbols) control vs time; (B) photocatalysis to photolysis ratio vs UV dose. Flow rate: 0.7 (black squares), 1.0 (red circles) and 5.0 mL min<sup>-1</sup> (blue triangles). The inset shows UV dose up to 200 mJ cm<sup>-2</sup>. (C) rate constant, Reynolds number and Zn<sup>2+</sup> concentration for each flow rate. Catalyst length 8.4 cm.

Single-pass tests showed complete CBZ degradation after only 30 min at both 0.7 and 1.0 mL min<sup>-1</sup> flow rates and consequently increased degradation kinetics

(cross ref Fig. 5b,c and Table 3). Enhanced overall quantum yields of 6.3×10<sup>-3</sup> and 5.6×10<sup>-3</sup> were achieved at lower flow rate conditions with enhanced kinetics (Table 3). The combination of longer photocatalytic foams and lower flow rates significantly improved quantum yield for single-pass studies as residence time and UV doses were greater than under recirculation conditions (Table S4 ESI). The quantum yield obtained for the photocatalytic foams in single pass configuration outperformed current systems, e.g. TiO<sub>2</sub> NPs suspensions [56, 57] and ZnO NPs suspensions [56, 59, 62] as well as immobilised TiO<sub>2</sub> [68] in batch reactors for CBZ removal. Although a higher quantum yield of 1.7×10<sup>-2</sup> was reported for ZnO suspensions in a batch reactor, energy consumption was 9 times higher than ZnO foams (Table 2) [61], while lower quantum yield and comparable energy consumption were obtained for another batch reactor with TiO<sub>2</sub> NPs [55] for CBZ photocatalytic degradation. A similar range of quantum yield values was reported for TiO<sub>2</sub> immobilised on glass rings (fixed-bed) and TiO<sub>2</sub> immobilised on flat substrates (fixed-film) respectively, in a batch recirculating system (150 W mercury lamp, 350 and 410 nm) for degradation of another pharmaceutical compound, clofibric acid [74]. ZnO foams achieved a higher quantum yield with lower energy consumption compared to TiO<sub>2</sub>/βSiC foams in batch [4, 75] and recirculating [76] [reactors and ZnFe<sub>2</sub>O<sub>4</sub>/Ni foam in batch [77] (cross ref Table 2 and Table S8 ESI). A higher quantum yield was achieved by ZnO/graphene composite foams, however, EEO was at least three orders of magnitude higher [78]. Quantum yields of ZnO photocatalytic foams were higher than reported for UV/H<sub>2</sub>O<sub>2</sub> CBZ degradation [66] and lower energy consumption than other advanced oxidation process as UV/H<sub>2</sub>O<sub>2</sub>, UV-LEDs/O<sub>3</sub> and UV/CI (Table S9 ESI) as discussed previously with inversely proportional correlations. The foams' surface area-to-volume ratio (SAV) has a particularly strong effect on the quantum yield (Table 3) as catalyst length was even higher than

531

532

533

534

535

536

537

538

539

540

541

542

543

544

545

546

547

548

549

550

551

552

553

554

recirculation. The energy efficiency at the lowest flow rate was comparable with values obtained for the recirculating system ( $E_{EO} = 36$  kWh m<sup>-3</sup>), whereas it increased by a factor of 5 for the 5 mL min<sup>-1</sup> condition (Table 3). These results demonstrate the ability of the foams to effectively capture light and improve reactivity.

**Table 3.** Quantum yield  $(\Phi)$  considering the foams' properties of external surface area (SA) and surface area-to-volume (SAV) as a function of flow rate, % CBZ removal, pseudo first order removal rate constant (k) and electrical energy per order (E<sub>EO</sub>) for single-pass reactor along with correlation. Catalyst length 8.4 cm. Photolysis quantum yield  $(\Phi_{photolysis})$ .

Degradation	Flow rate (mL min <sup>-1</sup> )	%CBZ removal	k.				normalised Φ	
conditions			(s <sup>-1</sup> )*	Φ <sub>photolysis</sub> Φ –		Φ/SA (m <sup>-2</sup> )	Φ/SAV (m)	_ E <sub>EO</sub> (kWh m <sup>-3</sup> )
	0.7	100	1.6×10 <sup>-3</sup>		6.3×10 <sup>-3</sup>	0.05	1.5×10 <sup>-6</sup>	36
photocatalysis	1.0	96	1.4×10 <sup>-3</sup>		5.6×10 <sup>-3</sup>	0.05	1.3×10 <sup>-6</sup>	125
	5.0	35	5.0×10 <sup>-4</sup>		1.9×10 <sup>-3</sup>	0.02	4.6×10 <sup>-7</sup>	187
	correlation	-	-0.994		-0.996	-0.998	-0.993	0.845
	0.7	87	2.5×10 <sup>-4</sup>	5.8×10 <sup>-5</sup>				
photolysis	1.0	62	1.8×10 <sup>-4</sup>	4.3×10 <sup>-5</sup>				
	5.0	9.0	1.3×10 <sup>-4</sup>	3.1×10 <sup>-5</sup>				

<sup>\*</sup> the associated error is < 10<sup>-3</sup>.

#### 3.4. Single-pass and recirculating reactors comparison

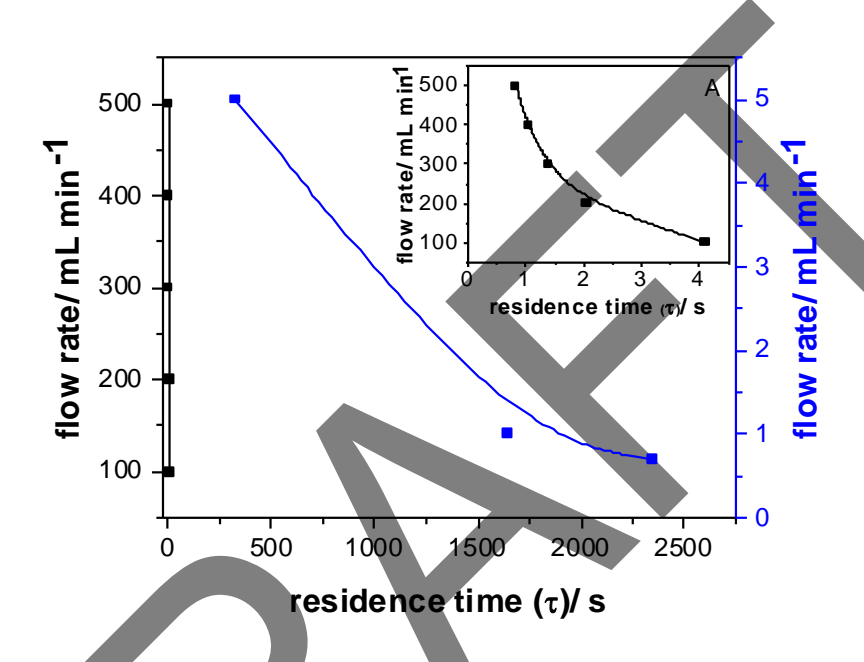
The single-pass configuration could be seen as a limiting case of the recirculating configuration as the flow rate decreases. Combining the kinetics in a single plot shows an inverse exponential correlation with Reynolds number (Fig. 6b). This is reflected in the significantly higher residence time (Fig. 6a) calculated for lower flow rates and fraction of illuminated volume over total volume (Table S3 ESI) being one order of magnitude higher for the single-pass to achieve similar CBZ degradation

Φ<sub>photolysis</sub> calculated from equations S10 and S11.

Φ calculated using equation S7.

 $<sup>\</sup>Phi_{\text{SAV}}$  calculated using equation S8 and S9.

compared to the recirculating configuration. Both characteristics translated in a significantly higher efficiency of the single pass configuration, which achieved complete degradation in 30 minutes, whereas the recirculating could obtain only 95% after 120 minutes of irradiation (Fig. 3c). A comparable kinetics ratio of photocatalysis/photolysis of 8.0 was observed for both studied reactor configurations.



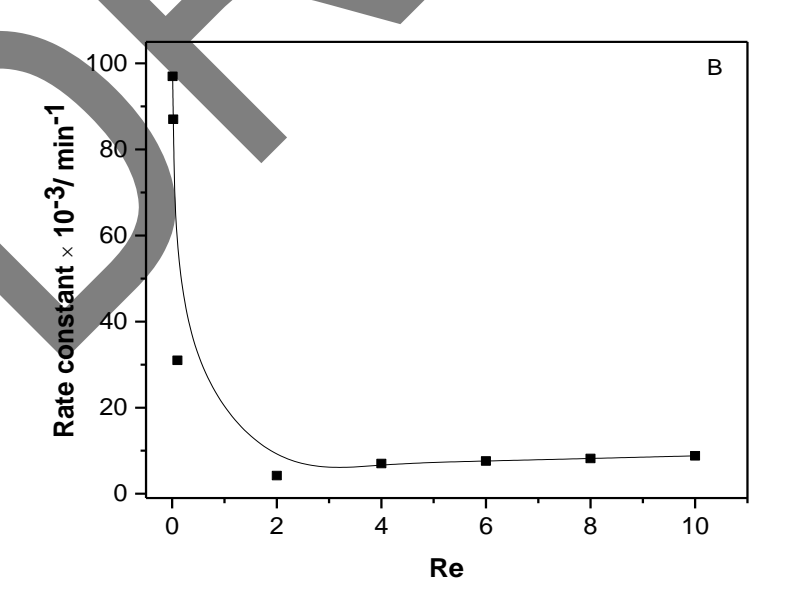


**Fig. 6.** Flow rate as a function of (A) residence time ( $\tau$ ) for recirculation (black squares) and single pass (blue squares) studies. The inset shows the recirculation profile at a lower scale; (B) rate constant vs. Reynolds number for both reactor configurations.

# 3.5. Scale-up considerations

Simulations of the single-pass configuration were conducted to investigate the potential for scale-up of the foams. The simulation results were performed considering the highest flow rate studied (5.0 mL min<sup>-1</sup>) for the single-pass reactor, showing that by increasing the catalyst length, degradation was significantly improved. An increase of catalyst length from 8.4 cm to 70.0 cm, increased single-pass degradation from 24 to 82% (cross ref Fig. 7 and Table S10 ESI) and reduced the  $E_{EO}$  from 187 to 47 kWh m<sup>-3</sup>. The simulated conversion results accounting for photocatalysis to photolysis contribution (Table S10 ESI) agreed with the experimental data. Pressure drop ( $\Delta$ P) values were negligible for catalyst lengths 8.4 and 70.0 cm (Table S11 ESI).

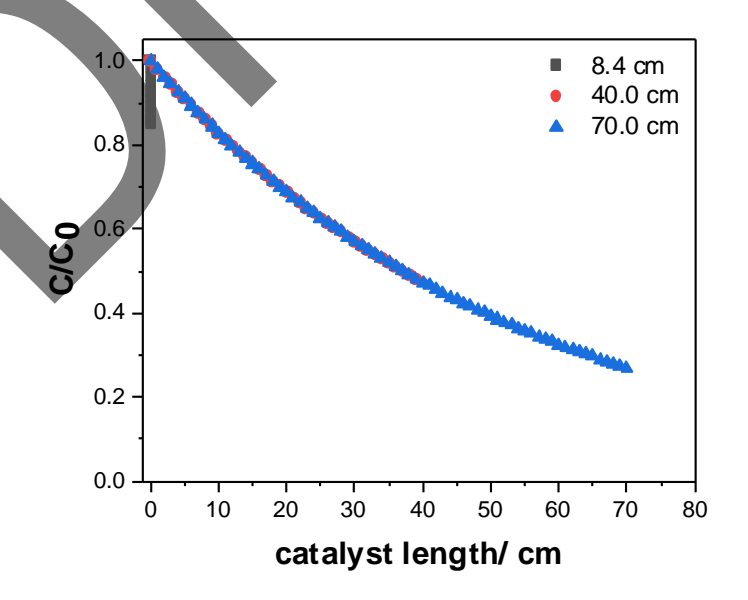


**Fig. 7.** Simulation results for CBZ photocatalytic degradation as a function of catalyst length for the single pass reactor.

The combination of longer, energy efficient 3D foams with higher flow rates in the single-pass configuration could open new perspectives towards the scaling-up of photocatalytic reactors. Removal of organic micropollutants with reduced operational costs was demonstrated especially eliminating the need for NPs downstream separation.

#### 4. Conclusions

ZnO photocatalytic foams prepared with 2-step sintering process demonstrated high photocatalytic activity and enhanced chemical and mechanical stability under continuous recirculating and single-pass conditions with low energy consumption. This sintering approach resulted in greater interconnected pores within the 3D structure. Improved photocatalytic degradation kinetics were associated to flow rates up to 200 mL min<sup>-1</sup>, increasing the foams' length significantly improved degradation kinetics and quantum yield up to 1.2×10<sup>-3</sup>, leading to 95% CBZ oxidation after 120 min. ZnO self-supporting foams were stable over 5 consecutive cycles of 2 hours each with improved chemical stability and linear correlation with catalyst length. Significantly low electrical energy per order (E<sub>EO</sub>) of 17 kwh m³ was consumed under recirculation conditions. The use of ZnO photocatalytic foams in recirculation reactors proved to be as energy efficient as other AOPs. Additionally, the photocatalytic activity of self-supporting ZnO foams in single-pass reactor was demonstrated for the first time. Complete CBZ removal with reduced energy consumption was achieved after only 30 min at 0.7 mL

min<sup>-1</sup> owing to increased kinetics and quantum yield (6.3×10<sup>-3</sup>) while proportionally reduced energy consumption. Exponential concentration decay was demonstrated as function of UV dose until reaching steady-state. Photo-corrosion resulted in dissolved Zn levels well below WHO drinking water guidelines. Simulation studies demonstrated high CBZ removal (82%) could be reached at 5.0 mL min<sup>-1</sup> for 70 cm catalyst length with reduced energy consumption. In both reactor configurations, the ZnO foams demonstrated high mechanical and chemical stability, low energy consumption and high quantum yields. These results demonstrate that the self-supporting ZnO photocatalytic foams have the potential to be scaled-up for use in wastewater treatment plants to remove of organic micropollutants, overcoming the limitations of current technology.

#### 5. Acknowledgements

The authors are grateful for EPSRC for funding support (Grant No. EP/P031382/1). The authors acknowledge the Material and Chemical Characterisation Facility (MC²) at the University of Bath. We are also grateful to Mr. Paul Frith for the technical support on the reactor design. The authors acknowledge James Andy Milton and the National Oceanography Centre Southampton at the University of Southampton for the Inductively Coupled Plasma Mass Spectrometry (ICP-MS) analysis. The authors acknowledge Dr. Daniel F. Segura for artwork support. All data produced during this research are available from the University of Bath open access data archive at (https://doi.org/10.15125/BATH-01116).

- [1] Who, Unicef, Progress on household drinking water, sanitation and hygiene, 2020.
- [2] EuropeanCommission, Decision (EU) 2020/1161 watch list of substances, 2020.
- 652 [3] T. Gallé, C. Koehler, M. Plattes, D. Pittois, M. Bayerle, R. Carafa, A. Christen, J.
- 653 Hansen, Large-scale determination of micropollutant elimination from municipal
- 654 wastewater by passive sampling gives new insights in governing parameters and
- 655 degradation patterns, Water Research 160 (2019) 380-393.
- 656 https://doi.org/10.1016/j.watres.2019.05.009.
- 657 [4] M. Rico-Santacruz, P. Garciá-Munoz, C. Marchal, N. Batail, C. Pham, D. Robert,
- N. Keller, Coating-free TiO<sub>2</sub>@β-SiC alveolar foams as a ready-to-use composite
- 659 photocatalyst with tunable adsorption properties for water treatment, RSC Advances
- 660 10(7) (2020) 3817-3825. https://doi.org/10.1039/c9ra09553e.
- [5] Z. Long, Q. Li, T. Wei, G. Zhang, Z. Ren, Historical development and prospects of
- 662 photocatalysts for pollutant removal in water, Journal of Hazardous Materials
- 395(April) (2020) 122599-122599. https://doi.org/10.1016/j.jhazmat.2020.122599.
- 664 [6] D.B. Miklos, C. Remy, M. Jekel, K.G. Linden, J.E. Drewes, U. Hübner, Evaluation
- of advanced oxidation processes for water and wastewater treatment A critical
- 666 review, Water Research 139 (2018) 118-131.
- 667 https://doi.org/10.1016/j.watres.2018.03.042.
- 668 [7] C.B. Ong, L.Y. Ng, A.W. Mohammad, A review of ZnO nanoparticles as solar
- 669 photocatalysts: Synthesis, mechanisms and applications, Renewable and Sustainable
- 670 Energy Reviews 81(August 2017) (2018) 536-551.
- 671 https://doi.org/10.1016/j.rser.2017.08.020.
- [8] Z. Xing, J. Zhang, J. Cui, J. Yin, T. Zhao, J. Kuang, Z. Xiu, N. Wan, W. Zhou, Recent
- 673 advances in floating TiO2-based photocatalysts for environmental application, Applied
- 674 Catalysis B: Environmental 225(August 2017) (2018) 452-467.
- 675 https://doi.org/10.1016/j.apcatb.2017.12.00
- 676 [9] S. Horikoshi, N. Serpone, Can the photocatalyst TiO2 be incorporated into a wastewater treatment method? Background and prospects, Catalysis Today
- 678 340(August 2018) (2020) 334-346. https://doi.org/10.1016/j.cattod.2018.10.020.
- [10] F.B. Elehinafe, O. Agboola, A.D. Vershima, G.O. Bamigboye, Insights on the advanced separation processes in water pollution analyses and wastewater treatment
- 681 A review, South African Journal of Chemical Engineering 42(April) (2022) 188-200.
- 682 https://doi.org/10.1016/j.sajce.2022.08.004.
- 683 [11] S. Ahmed, F.S.A. Khan, N.M. Mubarak, M. Khalid, Y.H. Tan, S.A. Mazari, R.R.
- 684 Karri, E.C. Abdullah, Emerging pollutants and their removal using visible-light
- 685 responsive photocatalysis A comprehensive review, Journal of Environmental
- 686 Chemical Engineering 9(6) (2021) 106643-106643.
- 687 https://doi.org/10.1016/j.jece.2021.106643.
- 688 [12] A.N. Kouamé, R. Masson, D. Robert, N. Keller, V. Keller, β-SiC foams as a
- 689 promising structured photocatalytic support for water and air detoxification, Catalysis
- 690 Today 209 (2013) 13-20. https://doi.org/10.1016/j.cattod.2012.12.008.
- 691 [13] P. She, S. Yin, Q. He, X. Zhang, K. Xu, Y. Shang, X. Men, S. Zeng, H. Sun, Z.
- 692 Liu, A self-standing macroporous Au/ZnO/reduced graphene oxide foam for recyclable
- 693 photocatalysis and photocurrent generation, Electrochimica Acta 246 (2017) 35-42.
- 694 https://doi.org/10.1016/j.electacta.2017.06.027.
- 695 [14] M. Martín-Sómer, C. Pablos, A. de Diego, R. van Grieken, Á. Encinas, V.M.
- 696 Monsalvo, J. Marugán, Novel macroporous 3D photocatalytic foams for simultaneous
- 697 wastewater disinfection and removal of contaminants of emerging concern, Chemical

- 698 Engineering Journal 366(November 2018) (2019)449-459.
- https://doi.org/10.1016/j.cej.2019.02.102. 699
- [15] T. Wang, C. Zhu, L. Song, P. Du, Y. Yang, J. Xiong, A facile controllable 700 701 preparation of highly porous carbon foam and its application in photocatalysis,
- 702 Research Bulletin 122(November 2019) (2020) 110697-110697.
- 703 https://doi.org/10.1016/j.materresbull.2019.110697.
- 704 [16] Y. Xue, R. Su, G. Zhang, Q. Wang, P. Wang, W. Zhang, Z. Wang, Visible light
- 705 responsive Fe-ZnS/nickel foam photocatalyst with enhanced photocatalytic activity
- stability, 706 **RSC** Advances 93370-93373. and 6(96) (2016)
- 707 https://doi.org/10.1039/c6ra20187c.
- [17] M. Kete, O. Pliekhova, L. Matoh, U.L. Stangar, Design and evaluation of a 708
- 709 compact photocatalytic reactor for water treatment, Environmental Science and
- 710 Pollution Research 25(21) (2018) 20453-20465. https://doi.org/10.1007/s11356-017-711 9895-3.
- [18] F. Cao, Z. Pan, X. Ji, Enhanced photocatalytic activity of a pine-branch-like ternary 712
- 713 CuO/CuS/ZnO heterostructure under visible light irradiation, New Journal of Chemistry
- 714 43(28) (2019) 11342-11347. https://doi.org/10.1039/c9nj01785b.
- 715 [19] S.W. da Silva, J.P. Bortolozzi, E.D. Banús, A.M. Bernardes, M.A. Ulla, TiO<sub>2</sub> thick
- 716 films supported on stainless steel foams and their photoactivity in the nonylphenol
- 717 ethoxylate mineralization, Chemical Engineering Journal 283 (2016) 1264-1272.
- 718 https://doi.org/10.1016/j.cej.2015.08.057.
- [20] K. Elatmani, N.B. oujji, G. Plantara, V. Goetz, I.A. ichou, 3D Photocatalytic media 719
- for decontamination of water from pesticides, Materials Research Bulletin 720
- 101(December 2017) (2018) 6-11. <a href="https://doi.org/10.1016/j.materresbull.2017.12.042">https://doi.org/10.1016/j.materresbull.2017.12.042</a>. [21] C.B.D. Marien, M. Le, A. Azaïs, I. Christian, M. Bra, P. Drogui, A. Dirany, D. 721
- 722
- 723 Robert, Kinetics and mechanism of Paraquat's degradation: UV-C photolysis vs UV-
- C photocatalysis with TiO2/SiC foams, Journal of Hazardous Materials 370(December 724
- 2017) (2019) 164-171. https://doi.org/10.1016/j.jhazmat.2018.06.009. 725
- [22] Z. Švagelj, V. Mandić, L. Ćurković, M. Biošić, I. Žmak, M. Gaborardi, Titania-726
- Coated alumina foam photocatalyst for memantine degradation derived by replica 727
- 728 sol-gel reaction, Materials method 13(1) (2020).
- 729 https://doi.org/10.3390/ma13010227.
- [23] T. Yildiz, H.C. Yatmaz, K. Öztürk, Anatase TiO<sub>2</sub> powder immobilized on reticulated 730
- 731 Al<sub>2</sub>O<sub>3</sub> ceramics as a photocatalyst for degradation of RO16 azo dye, Ceramics
- 732 International 46(7) (2020) 8651-8657. https://doi.org/10.1016/j.ceramint.2019.12.098.
- 733 [24] Y.F. Zhu, L. Zhou, Q.S. Jiang, One-dimensional ZnO nanowires grown on three-
- dimensional scaffolds for improved photocatalytic activity, Ceramics International 734
- 735 46(1) (2020) 1158-1163. https://doi.org/10.1016/j.ceramint.2019.09.084.
- 736 [25] A. Kocakuşakoğlu, M. Dağlar, M. Konyar, H.C. Yatmaz, K. Öztürk, Photocatalytic
- activity of reticulated ZnO porous ceramics in degradation of azo dye molecules, 737
- 738 Journal the European Ceramic Society 35(10) (2015)2845-2853.
- 739 https://doi.org/10.1016/i.jeurceramsoc.2015.03.042.
- 740 [26] Y. Zhang, L. Liu, B. Van der Bruggen, M.K.H. Leung, F. Yang, A free-standing 3D
- 741 nano-composite photo-electrode—Ag/ZnO nanorods arrays on Ni foam effectively
- 742 degrade berberine, Chemical Engineering Journal 373(October 2018) (2019) 179-191.
- 743 https://doi.org/10.1016/j.cej.2019.05.026.
- 744 [27] M. Song, K. Qi, Y. Wen, X. Zhang, Y. Yuan, X. Xie, Z. Wang, Rational design of
- 745 novel three-dimensional reticulated Ag2O/ZnO Z-scheme heterojunction on Ni foam
- 746 for promising practical photocatalysis, Science of the Total Environment 793 (2021)
- 747 148519-148519. https://doi.org/10.1016/j.scitotenv.2021.148519.

- 748 [28] T.T. Guaraldo, J. Wenk, D. Mattia, Photocatalytic ZnO Foams for Micropollutant
- 749 Degradation, Advanced Sustainable Systems 5(5) (2021) 2000208.
- 750 https://doi.org/10.1002/adsu.202000208.
- 751 [29] K.M. Lee, C.W. Lai, K.S. Ngai, J.C. Juan, Recent developments of zinc oxide
- based photocatalyst in water treatment technology: A review, Water Research 88
- 753 (2016) 428-448. <a href="https://doi.org/10.1016/j.watres.2015.09.045">https://doi.org/10.1016/j.watres.2015.09.045</a>.
- 754 [30] C. Martínez, M. Canle L, M.I. Fernández, J.A. Santaballa, J. Faria, Kinetics and
- 755 mechanism of aqueous degradation of carbamazepine by heterogeneous
- 756 photocatalysis using nanocrystalline TiO2, ZnO and multi-walled carbon nanotubes-
- 757 anatase composites, Applied Catalysis B: Environmental 102(3-4) (2011) 563-571.
- 758 https://doi.org/10.1016/j.apcatb.2010.12.039.
- 759 [31] L. Haroune, M. Salaun, A. Ménard, C.Y. Legault, J.-p. Bellenger, Photocatalytic
- degradation of carbamazepine and three derivatives using TiO2 and ZnO: Effect of
- pH, ionic strength, and natural organic matter, Science of The Total Environment 475 (2014) 16-22. https://doi.org/10.1016/j.scitotenv.2013.12.104.
- 762 (2014) 10-22. https://doi.org/10.1010/j.scitotenv.2013.122104.
- 764 corrosion resistance of ZnO nanowire photocatalysts, Journal of Hazardous Materials
- 765 378(June) (2019) 120799-120799. https://doi.org/10.1016/j.jhazmat.2019.120799.
- 766 [33] I.J. Ochuma, O.O. Osibo, R.P. Fishwick, S. Pollington, A. Wagland, J. Wood, J.M.
- 767 Winterbottom, Three-phase photocatalysis using suspended titania and titania
- supported on a reticulated foam monolith for water purification, Catalysis Today 128(1-
- 769 2 SPEC. ISS.) (2007) 100-107. https://doi.org/10.1016/j.cattod.2007.05.015.
- 770 [34] I.C. M'Bra, P. García-Muñoz, P. Drogui, N. Keller, A. Trokourey, D. Robert,
- 771 Heterogeneous photodegradation of Pyrimethanil and its commercial formulation with
- 772 TiO<sub>2</sub> immobilized on SiC foams, Journal of Photochemistry & Photobiology, A:
- 773 Chemistry 368(July 2018) (2019) 1-6.
- 774 https://doi.org/10.1016/j.jphotochem.2018.09.007.
- 775 [35] A. Uricchio, E. Nadal, B. Plujat, G. Plantard, F. Massines, F. Fanelli, Low-
- temperature atmospheric pressure plasma deposition of TiO<sub>2</sub>-based nanocomposite coatings on open-cell polymer foams for photocatalytic water treatment, Applied
- 777 Coatings on open cent polymer loams for photocatalytic water treatment, Applied 778 Surface Science 561(January) (2021) 150014-150014.
- 779 https://doi.org/10.1016/j.apsusc.2021.150014.
- 780 [36] J.L. Wilkinson, A.B.A. Boxall, D.W. Kolpin, K.M.Y. Leung, R.W.S. Lai, D. Wong,
- 781 R. Ntchantcho, J. Pizarro, J. Mart, S. Echeverr, J. Garric, A. Chaumot, P. Gibba, I.
- 782 Kunchulia, S. Seidensticker, G. Lyberatos, J.M. Morales-salda, H. Kang,
- 783 Pharmaceutical pollution of the world 's rivers, PNAS 119(8) (2022) 1-10.
- https://doi.org/10.1073/pnas.2113947119/-/DCSupplemental.Published.
- 785 [37] B.A. Wols, C.H.M. Hofman-Caris, Review of photochemical reaction constants of
- organic micropollutants required for UV advanced oxidation processes in water, Water
- 787 Research 46(9) (2012) 2815-2827. https://doi.org/10.1016/j.watres.2012.03.036.
- 788 [38] W.L. Wang, Q.Y. Wu, N. Huang, Z.B. Xu, M.Y. Lee, H.Y. Hu, Potential risks from
- 789 UV/H2O2 oxidation and UV photocatalysis: A review of toxic, assimilable, and
- 790 sensory-unpleasant transformation products, Water Research 141 (2018) 109-125.
- 791 https://doi.org/10.1016/j.watres.2018.05.005.
- 792 [39] M. Mazaheri, A.M. Zahedi, S.K. Sadrnezhaad, Two-step sintering of
- 793 nanocrystalline ZnO compacts: Effect of temperature on densification and grain
- 794 growth, Journal of the American Ceramic Society 91(1) (2008) 56-63.
- 795 https://doi.org/10.1111/j.1551-2916.2007.02029.x.

- 796 [40] N.J. Lóh, L. Simão, C.A. Faller, A. De Noni, O.R.K. Montedo, A review of two-step
- 797 sintering for ceramics, Ceramics International 42(11) (2016) 12556-12572.
- https://doi.org/10.1016/j.ceramint.2016.05.065. 798
- 799 [41] Y. Liao, R. Wang, M. Tian, C. Qiu, A.G. Fane, Fabrication of polyvinylidene
- 800 fluoride (PVDF) nanofiber membranes by electro-spinning for direct contact
- membrane distillation, Journal of Membrane Science 425-426(11) (2013) 30-39. 801
- 802 https://doi.org/10.1016/j.memsci.2012.09.023.
- 803 [42] S.A.M. Karimian, A.G. Straatman, CFD study of the hydraulic and thermal
- 804 behavior of spherical-void-phase porous materials, International Journal of Heat and
- 805 Fluid Flow 29(1) (2008) 292-305. https://doi.org/10.1016/j.ijheatfluidflow.2007.07.003.
- 806 [43] S.E. Braslavsky, Glossary of terms used in photochemistry 3rd edition: (IUPAC
- Recommendations 2006), Pure and Applied Chemistry 79(3) (2007) 293-465. 807
- 808 https://doi.org/10.1351/pac200779030293.
- [44] J.R. Bolton, K.G. Bircher, W. Tumas, C.A. Tolman, Figures-of-merit for the 809
- 810 technical development and application of advanced technologies for both electric- and
- 811 Pure and Applied Chemistry 73 (2001) systems,
- https://doi.org/10.1351/pac200173040627. 812
- [45] A. Mirzaei, L. Yerushalmi, Z. Chen, F. Haghighat, J. Guo, Enhanced photocatalytic 813
- degradation of sulfamethoxazole by zinc oxide photocatalyst in the presence of 814
- fluoride ions: Optimization of parameters and toxicological evaluation, Water Research 132 (2018) 241-251. <a href="https://doi.org/10.1016/j.watres.2018.01.016">https://doi.org/10.1016/j.watres.2018.01.016</a>. 815
- 816
- 817 [46] S. Ibadat, M. Younas, S. Shahzada, M. Nadeem, T. Ali, M.J. Akhtar, S. Pollastri,
- U.U. Rehman, I. Yousef, R.T. Ali Khan, Realistic dielectric response of high 818
- temperature sintered ZnO ceramic: A microscopic and spectroscopic approach, RSC 819
- Advances 10(51) (2020) 30451-30462. https://doi.org/10.1039/d0ra04273k. 820
- 821 [47] X. Jiang, G. Zhu, H. Xu, L. Dong, J. Song, X. Zhang, Y. Zhao, D. Yan, A. Yu,
- Preparation of high density ZnO ceramics by the Cold Sintering Process, Ceramics 822
- 823 International 45(14) 17382-17386. (2019)
- https://doi.org/10.1016/j.ceramint.2019.05.298. 824
- [48] J. Wang, Z. Wang, B. Huang, Y. Ma, Y. Liu, X. Qin, X. Zhang, Y. Dai, Oxygen 825
- 826 vacancy induced band-gap narrowing and enhanced visible light photocatalytic activity
- 827 of ZnO, ACS Applied Materials and Interfaces 4(8) (2012) 4024-4030.
- https://doi.org/10.1021/am300835p. 828
- 829 [49] D.P. Mohapatra, S.K. Brar, R. Daghrir, R.D. Tyagi, P. Picard, R.Y. Surampalli, P.
- 830 Drogui, Photocatalytic degradation of carbamazepine in wastewater by using a new
- 831 class of whey-stabilized nanocrystalline TiO2 and ZnO, Science of the Total
- 832 Environment 485-486(1) (2014)263-269.
- https://doi.org/10.1016/j.scitotenv.2014.03.089. 833
- [50] D.B. Miklos, R. Hartl, P. Michel, K.G. Linden, J.E. Drewes, U. Hübner, UV/H2O2 834
- 835 process stability and pilot-scale validation for trace organic chemical removal from
- 836 wastewater treatment plant effluents, Water Research 136 (2018) 169-179.
- https://doi.org/10.1016/j.watres.2018.02.044. 837
- [51] Q. Wang, H. Zhou, X. Liu, T. Li, C. Jiang, W. Song, W. Chen, Facet-dependent 838
- 839 generation of superoxide radical anions by ZnO nanomaterials under simulated solar
- 840 Environmental Science: Nano 5(12) (2018)2864-2875.
- https://doi.org/10.1039/c8en01008k. 841
- [52] H. de Lasa, B. Serrano, M. Salaices, Photocatalytic Reaction Engineering, 842
- 843 Springer US, New York, 2005. https://doi.org/10.1007/0-387-27591-6.

- 844 [53] S. Wang, Z. Cheng, L. Jiang, Y. Song, Y. Liu, Quantitative study of density-driven
- convection mass transfer in porous media by MRI, Journal of Hydrology 594(July
- 846 2020) (2021) 125941-125941. https://doi.org/10.1016/j.jhydrol.2020.125941.
- 847 [54] C.Q. Wu, H.J. Xu, C.Y. Zhao, A new fractal model on fluid flow/heat/mass
- 848 transport in complex porous structures, International Journal of Heat and Mass
- 849 Transfer 162 (2020). <a href="https://doi.org/10.1016/j.ijheatmasstransfer.2020.120292">https://doi.org/10.1016/j.ijheatmasstransfer.2020.120292</a>.
- 850 [55] A. Jelic, I. Michael, A. Achilleos, E. Hapeshi, D. Lambropoulou, S. Perez, M.
- 851 Petrovic, D. Fatta-Kassinos, D. Barcelo, Transformation products and reaction
- pathways of carbamazepine during photocatalytic and sonophotocatalytic treatment,
- 853 Journal of Hazardous Materials 263 (2013) 177-186.
- 854 https://doi.org/10.1016/j.jhazmat.2013.07.068.
- 855 [56] I. Georgaki, E. Vasilaki, N. Katsarakis, A Study on the Degradation of
- 856 Carbamazepine and Ibuprofen by TiO2 & ZnO Photocatalysis upon UV/Visible-Light
- 857 Irradiation, American Journal of Analytical Chemistry 05(08) (2014) 518-534.
- 858 <a href="https://doi.org/10.4236/ajac.2014.58060">https://doi.org/10.4236/ajac.2014.58060</a>.
- 859 [57] A. Surenjan, B. Sambandam, T. Pradeep, L. Philip, Synthesis, characterization
- and performance of visible light active C-TiO2 for pharmaceutical photodegradation,
- 861 Journal of Environmental Chemical Engineering 5(1) (2017) 757-767
- 862 https://doi.org/10.1016/j.jece.2016.12.044.
- 863 [58] N.F.F. Moreira, M.J. Sampaio, A.R. Ribeiro, C.G. Silva, J.L. Faria, A.M.T. Silva,
- 864 Metal-free g-C3N4 photocatalysis of organic micropollutants in urban wastewater
- under visible light, Applied Catalysis B: Environmental 248(August 2018) (2019) 184-
- 866 192. <a href="https://doi.org/10.1016/j.apcatb.2019.02.001">https://doi.org/10.1016/j.apcatb.2019.02.001</a>.
- 867 [59] N.P.F. Gonçalves, M.A.O. Lourenço, S.R. Baleuri, S. Bianco, P. Jagdale, P.
- 868 Calza, Biochar waste-based ZnO materials as highly efficient photocatalysts for water
- 869 treatment, Journal of Environmental Chemical Engineering 10(2) (2022) 107256-
- 870 107256. https://doi.org/10.1016/j.jece.2022.107256.
- 871 [60] Y. Zhang, D. Li, Y. Zhang, X. Zhou, S. Guo, L. Yang, Graphene-wrapped
- 872 Bi2O2CO3 core-shell structures with enhanced quantum efficiency profit from an
- 873 ultrafast electron transfer process, Journal of Materials Chemistry A 2(22) (2014)
- 874 8273-8280. https://doi.org/10.1039/c4ta00088a.
- 875 [61] S. Teixeira, R. Gurke, H. Eckert, K. Kühn, J. Fauler, G. Cuniberti, Photocatalytic
- 876 degradation of pharmaceuticals present in conventional treated wastewater by
- 877 nanoparticle suspensions, Journal of Environmental Chemical Engineering 4(1)
- 878 (2016) 287-292. https://doi.org/10.1016/j.jece.2015.10.045.
- 879 [62] H. Mohan, V. Ramalingam, A. Adithan, K. Natesan, K.K. Seralathan, T. Shin,
- 880 Highly efficient visible light driven photocatalytic activity of zinc/ferrite: Carbamazepine
- degradation, mechanism and toxicity assessment, Journal of Hazardous Materials
- 882 416(May) (2021) 126209-126209. https://doi.org/10.1016/j.jhazmat.2021.126209.
- 883 [63] K. Zhang, W. Zhou, X. Zhang, B. Sun, L. Wang, K. Pan, B. Jiang, G. Tian, H. Fu,
- 884 Self-floating amphiphilic black TiO2 foams with 3D macro-mesoporous architectures
- as efficient solar-driven photocatalysts, Applied Catalysis B: Environmental 206 (2017)
- 886 336-343. https://doi.org/10.1016/j.apcatb.2017.01.059.
- 887 [64] X. Men, H. Chen, K. Chang, X. Fang, C. Wu, W. Qin, S. Yin, Three-dimensional
- 888 free-standing ZnO/graphene composite foam for photocurrent generation and
- 889 photocatalytic activity, Applied Catalysis B: Environmental 187 (2016) 367-374.
- 890 https://doi.org/10.1016/j.apcatb.2016.01.052.
- 891 [65] Z. Warren, T.T. Guaraldo, J. Wenk, D. Mattia, Synthesis of Photocatalytic Pore
- 892 Size-Tuned ZnO Molecular Foams, Journal of Materials Chemistry A (2022).
- 893 https://doi.org/10.1039/D2TA02038F.

- 894 [66] B.A. Wols, D.J.H. Harmsen, J. Wanders-Dijk, E.F. Beerendonk, C.H.M. Hofman-
- 895 Caris, Degradation of pharmaceuticals in UV (LP)/H2O2 reactors simulated by means
- of kinetic modeling and computational fluid dynamics (CFD), Water Research 75(0)
- 897 (2015) 11-24. <a href="https://doi.org/10.1016/j.watres.2015.02.014">https://doi.org/10.1016/j.watres.2015.02.014</a>.
- 898 [67] J. Bohdziewicz, E. Kudlek, M. Dudziak, Influence of the catalyst type (TiO2 and
- 899 ZnO) on the photocatalytic oxidation of pharmaceuticals in the aquatic environment,
- 900 Desalination and Water Treatment 57(3) (2014) 1552-1563.
- 901 https://doi.org/10.1080/19443994.2014.988411.
- 902 [68] Y. He, N.B. Sutton, H.H.H. Rijnaarts, A.A.M. Langenhoff, Degradation of
- 903 pharmaceuticals in wastewater using immobilized TiO<sub>2</sub> photocatalysis under
- 904 simulated solar irradiation, Applied Catalysis B: Environmental 182 (2016) 132-141.
- 905 https://doi.org/10.1016/j.apcatb.2015.09.015.
- 906 [69] D. Avisar, I. Horovitz, L. Lozzi, F. Ruggieri, M. Baker, M.L. Abel, H. Mamane,
- 907 Impact of water quality on removal of carbamazepine in natural waters by N-doped
- 908 TiO2 photo-catalytic thin film surfaces, Journal of Hazardous Materials 244-245 (2013)
- 909 463-471. https://doi.org/10.1016/j.jhazmat.2012.09,058.
- 910 [70] S. Carbonaro, M.N. Sugihara, T.J. Strathmann, Continuous-flow photocatalytic
- 911 treatment of pharmaceutical micropollutants: Activity, inhibition, and deactivation of
- 912 TiO<sub>2</sub> photocatalysts in wastewater effluent, Applied Catalysis B: Environmental 129
- 913 (2013) 1-12. https://doi.org/10.1016/j.apcatb.2012.09.014
- 914 [71] I. Horovitz, D. Avisar, M.A. Baker, R. Grilli, L. Lozzi, D. Di Camillo, H. Mamane,
- 915 Carbamazepine degradation using a N-doped TiO2 coated photocatalytic membrane
- 916 reactor: Influence of physical parameters, Journal of Hazardous Materials 310 (2016)
- 917 98-107. <a href="https://doi.org/10.1016/j.jhazmat.2016.02.008">https://doi.org/10.1016/j.jhazmat.2016.02.008</a>.
- 918 [72] T.T. Vu, L. del Río, T. Valdés-Solís, G. Marbán, Fabrication of wire mesh-
- supported ZnO photocatalysts protected against photocorrosion, Applied Catalysis B: Environmental 140-141 (2013) 189-198. <a href="https://doi.org/10.1016/j.apcatb.2013.04.023">https://doi.org/10.1016/j.apcatb.2013.04.023</a>.
- 921 [73] WHO, Joint Monitoring Programme for Water Supply and Sanitation, 2012.
- 922 [74] A. Manasserø, M.L. Satuf, O.M. Alfano, Photocatalytic reactors with suspended
- 923 and immobilized TiO2: Comparative efficiency evaluation, Chemical Engineering
- 924 Journal 326 (2017) 29-36. https://doi.org/10.1016/j.cej.2017.05.087.
- 925 [75] N.A. Kouamé, D. Robert, V. Keller, N. Keller, C. Pham, P. Nguyen, Preliminary
- 926 study of the use of β-SiC foam as a photocatalytic support for water treatment,
- 927 Catalysis Today 161(1) (2011) 3-7. https://doi.org/10.1016/j.cattod.2010.10.045.
- 928 [76] N.A. Kouamé, D. Robert, V. Keller, N. Keller, C. Pham, P. Nguyen, TiO2/β-SiC
- 929 foam-structured photoreactor for continuous wastewater treatment, Environmental
- 930 Science and Pollution Research 19(9) (2012) 3727-3734.
- 931 https://doi.org/10.1007/s/1356-011-0719-6.
- 932 [77] G. Zhang, Y. Xue, Q. Wang, P. Wang, H. Yao, W. Zhang, J. Zhao, Y. Li,
- 933 Photocatalytic oxidation of norfloxacin by Zn0.9Fe0.1S supported on Ni-foam under
- 934 visible light irradiation, Chemosphere 230 (2019) 406-415.
- 935 https://doi.org/10.1016/i.chemosphere.2019.05.015.
- 936 [78] M.M. Messina, M.E. Coustet, J. Ubogui, R. Ruiz, F.D. Saccone, P.C. Dos Santos
- 937 Claro, F.J. Ibañez, Simultaneous Detection and Photocatalysis Performed on a 3D
- 938 Graphene/ZnO Hybrid Platform, Langmuir 36(9) (2020) 2231-2239.
- 939 https://doi.org/10.1021/acs.langmuir.9b03502.